Recent glacier mass balance and area changes in the Kangri Karpo Mountains derived from multi-sources of DEMs and glacier inventories

Wu Kunpeng [1, 2], Liu Shiyin [2, 3*], Jiang Zongli [4], Xu Junli [5], Wei Junfeng [4], Guo Wanqin [2]

[1]School of Resources and Environment, Anqing Normal University, Anqing, Anhui, China

[2]State key Laboratory of Cryospheric Sciences, Northwest Institute of Eco-Environment and Resources, Chinese Academy of Sciences, Lanzhou, China

[3]Institute of International Rivers and Eco-Security, Yunnan University, Yunnan, China

[4]Department of Geography, Hunan University of Science and Technology, Xiangtan, China

[5]Department of Surveying and Mapping, Yancheng Teachers University, Yancheng, China

Correspondence to LIU Shiyin at liusy@lzb.ac.cn or WU Kunpeng at wukunpeng2008@lzb.ac.cn

Abstract. Due to the effect of Indian monsoon, the Kangri Karpo Mountains, located in southeast Tibetan Plateau, are the most humid region of Tibetan Plateau, and become one of the most important and concentrated regions with maritime (temperate) glaciers development. Glacier mass loss in Kangri Karpo Mountains is important contributor to global mean sea level rise, and it changes runoff distribution, increases risk of glacial lake outburst floods (GLOFs). Because of their difficult accessibility and high labor costs, the knowledge of glaciological parameters of glaciers in the Kangri Karpo Mountains is still limited. This study presents glacier elevation changes in the Kangri Karpo Mountains, by utilizing geodetic methods based on digital elevation models (DEM) derived from Topographic Maps (1980), the Shuttle Radar Topography Mission (SRTM) DEM (2000), and TerraSAR-X/TanDEM-X (2014). Glacier area and length changes were derived from Topographical Maps and Landsat TM/ETM+/OLI images between 1980 and 2015. Our results show that the Kangri Karpo Mountains contain 1166 glaciers, with an area of 2048.50 $\pm$48.65 km^2 in 2015. Ice cover in the Kangri Karpo Mountains diminished by 679.51 $\pm$59.49 km^2 (24.9% $\pm$2.2%) or 0.71% $\pm$0.06% a^{-1} from 1980 – 2015, however, with nine glaciers in advance from 1980–2015. Glaciers with area of 788.28 km^2 in the region, as derived from DEM differencing, have experienced a mean mass loss of 0.46 $\pm$ 0.08 m w.e. a^{-1} from 1980 – 2014. These glaciers showed slight accelerated shrinkage and significant accelerated mass loss during 2000 – 2015 compared to that during 1980 – 2000, which is consistent with the tendency of climate warming.

1 Introduction

Glaciers in the Tibetan Plateau (TP), as a key components in cryosphere system (Li et al., 2008), are the water resource of many major rivers and lakes (Immerzeel et al., 2010). Glacier mass balance is a valuable indicator to understand the climate variability on the TP (Oerlemans, 1994; Yao et al., 2012a). Under the background of global warming, many mountains glaciers have progressively shrunk in mass and extent in past decades (IPCC, 2013). However, glaciers with positive mass balance have also been reported in recent years, especially in the central Karakoram, eastern Pamir and the western TP (Bao et al., 2015; Gardelle et al., 2012b; Gardelle et al., 2013;

Kääb et al., 2015; Neckel et al., 2014; Yao et al., 2012a). The relationship between glacier mass balance and climate change, and the knowledge of water source in cryosphere and its disaster risks, are become an advanced research hotspot.

Glaciers in the Kangri Karpo Mountains are known as temperate characteristic under a warming climate and abundant precipitation from Indian Monsoon (Li et al., 1986; Shi and Liu, 2000). Based on digitized glacier inventories from Topographic Maps and remote sensing images, or in situ measurements, glaciers in the Kangri Karpo Mountains have experienced an intense area reduction, continued terminus retreat from 1980 – 2013, and mass deficit from 2005 – 2009 (Li et al., 2014; Yang et al., 2010; Yang et al., 2008; Yao et al., 2012a). While some previous studies showed that the phenomenon of glacier advance exists in the Kangri Karpo Mountains. Based on aerial photographs, China – Brazil Earth Resources Satellite (CBERS) image and Landsat Thematic Mapper (TM) image, about 60% of glaciers in the region have been losing their mass and other glaciers have advanced during 1980 to 2001 (Liu et al., 2006). Shi et al. (2006) attributed the complex behavior of glacier dynamics to the increase of precipitation suppressing glacier melting.

Previous studies have agreed that glaciers in the Kangri Karpo Mountains have experienced mass deficit, nevertheless, the results did differ from each other (Gardelle et al., 2013; Gardner et al., 2013; Kääb et al., 2015; Neckel et al., 2014). Using SRTM DEM and SPOT5 DEM (24 November 2011), glaciers experienced a mean thinning of 0.39 ± 0.16 m a^{-1} in the Kangri Karpo Mountains (Gardelle et al., 2013). Based on ICESat and SRTM, Kääb et al. (2015), Neckel et al. (2014) and Gardner et al. (2013) acquired different results over the Kangri Karpo Mountains, with glacier thickness loss of 1.34 ± 0.29 m a^{-1}, 0.81 ± 0.32 m a^{-1} and 0.30 ± 0.13 m a^{-1} during 2003 to 2009, respectively.

Glacier mass balance can be acquired through glaciological, hydrological and geodetic methods (Ye et al., 2015). Due to high altitude and harsh climatic conditions, it is hard to carry out widespread in-situ measurements. Meanwhile, satellite remote sensing is a promising alternative to conduct glacier mass balance through geodetic method, even in remote mountainous terrains and over several glaciers at a time (Paul and Haeberli, 2008). Glaciers in the Kangri Karpo Mountains were almost completely mapped by Topographic Maps that made from aerial photographs in October 1980, and then mapped by X-band SAR Interferometry (InSAR) in February 2000 during the SRTM resulting in a Digital Elevation Model. Glaciers in the region were mapped again by single-pass X-band InSAR from TerraSAR-X on 18 February 2014 and 13 March 2014, and its add-on for digital elevation measurements (TanDEM-X) (Krieger et al., 2007). In this study, the approach of Differential Synthetic Aperture Radar Interferometry (DInSAR) was used to estimate glacier mass balance in the Kangri Karpo Mountains between 1980 and 2014.

2 Study Area

The Kangri Karpo Mountains, located on the eastern end of the Nyainqentanglha Mountains in southeast Tibetan Plateau, extent about 280 km from northwest to southeast. This region is located in the south of Bomi County, and near to Motuo, Zayu and Basu County (Fig. 1). The north of this region, Purlung Zangbo, is a tributary of the Yalung Zangbo River, and the other side is Gongri Gabo River which belongs to west tributary of the Zayu River. Because the east section faces the entrance of the moist southwest monsoon from Indian Ocean, which enters into the plateau at the Grand Bend of the Yarlung Zangbo River, and the terrain forces the air flow to rise, it is the region with the maximum precipitation and highest moisture on the plateau and hence glaciers are

well-developed (Shi et al., 2008a).

During winter and spring, the westerly jet in the Northern Hemisphere is blocked by Tibetan Plateau and divided into two branches; southern branch develops into a trough in study area after bypassing the Himalaya Mountains. Moisture in the Bay of Bengal region is attracted by the trough, land on TP and form strong snowfall. In summer, due to the effect of topography flattening, abundant precipitation is transported to study area by the Indian monsoon (Li et al., 1986). Hence, the Kangri Karpo Mountains are the most humid region of Tibetan Plateau, and become one of the most important and concentrated regions with maritime (temperate) glaciers development (Shi and Liu, 2000). It is estimated that the mean summer air temperature at the equilibrium-line altitude (ELA) of glaciers in the region is usually above 1 ℃, and annual precipitation is about 2500–3000 mm (Shi et al., 1988). Most glaciers in study area are in the state of pressure melting point, glacier surface ablation is intensive and the velocity of glacier movement is fast (Li et al., 1986). Due to the large ablation and accumulation rates in this maritime region, glacier mass turnover is large in the Kangri Karpo Mountains.

According to the first Chinese Glacier Inventory, the Kangri Karpo Mountains contain 1320 glaciers, with a total area and volume of 2655.2 km^2 and 260.3 km^3, respectively (Mi et al., 2002). Yalong Glacier (CGI code: 5O282B37) is the largest one among these glaciers (191.4 km^2 in surface area and 32.5 km in length), while the Ata Glacier (CGI code: 5O291B181), located on the south slope of the Kangri Karpo Mountains, is the glacier with the lowest terminus at 2450 m, 16.7 km in length and 13.75 km^2 in area (Liu et al., 2006). Comparison of photographs taken in different time found that tongue position of Ata Glacier, ice volume and glacial surface conditions have changed greatly in the past decades (Yang et al., 2008).

3 Data

3.1 Topographic Maps

Five topographic maps on 1:100000 scale and fifty topographic maps on 1:50000 scale generated from aerial photos acquired in October 1980 by the Chinese Military Geodetic Service was employed in the present study. Using a seven parameter transformation method, these maps georeferenced into the 1954 Beijing Geodetic Coordinate System (BJ54) with geoid (datum level is Yellow Sea mean sea level at Qingdao Tidal Observatory in 1956) were re-projected into World Geodetic System 1984 (WGS1984)/Earth Gravity Model 1996 (EGM96) (Xu et al., 2013). The contour lines of the maps were manually digitized and then converted into raster DEM (TOPO DEM) with a 30 m grid cell by employing the Thiessen polygon method (Shangguan et al., 2010; Wei et al., 2015b; Zhang et al., 2016a). According to the national photogrametrical standard issued by the Standardization Administration of the People's Republic of China (GB/T12343.1, 2008), the nominal vertical accuracies of these topographic maps were controlled within 3-5 m for the flat (with slopes < 2 °) and hilly areas (with slope 2-6 °) and controlled within 8-14 m for the mountain (with slope 6-25 °) and high mountain areas (with slope >25 °). Since the slopes of the most of the glacierized areas in the Kangri Karpo Mountains were gentle (~19 °), the vertical accuracy of the TOPO DEM is better than 9 m on glaciers.

3.2 Shuttle Radar Topography Mission

The SRTM was conducted to acquire interferometric synthetic aperture radar (InSAR) date simultaneously in the C-band and X-band frequencies from 11 to 22 February 2000 (Farr et al.,

2007). The SRTM DEM can be referred to the glacier surface in the last balance year (1999) with slight seasonal variances (Gardelle et al., 2013; Pieczonka et al., 2013; Zwally et al., 2011). The X-band SAR system was operated with a swath width of 45 km leaving large data gaps in the resulting X-band DEM (Rabus et al., 2003). Unfortunately, only 23% of the Kangri Karpo glaciers are covered by the data set. The unfilled finished SRTM C-band DEM, with a swath width of 225 km and 1 arc-second resolution (approximately 30 m) in WGS84/EGM96, is freely available for scientific purposes (http://earthexplorer.usgs.gov/). Hence, the unfilled finished SRTM C-band DEM was employed to study ice surface elevation change.

3.3 TerraSAR-X/TanDEM-X

TerraSAR-X was launched in June 2007 by the German Aerospace Center (DLR). TerraSAR-X and its add-on for digital elevation measurements (TanDEM-X) are flying in a close orbit formation acting as a flexible single-pass SAR interferometer (Krieger et al., 2007). Interferometric data acquisition can be performed in the pursuit monostatic mode, the bistatic mode and the alternating bistatic mode. Current baseline for operational DEM generation is the bistatic mode which minimizes temporal decorrelation and makes efficient use of the transmit power (Krieger et al., 2007).

The experimental Co-registered Single look Slant range Complex (CoSSC) files, acquired in bistatic InSAR stripmap mode on 18 February 2014 and 13 March 2014, were employed in this study (Fig. 2 and Table 1). The CoSSC files have been focused and co-registered at the TanDEM-X Processing and Archiving Facility (PAF). The GAMMA SAR and interferometric processing software was employed for the interferometric processing of the CoSSC files (Werner et al., 2000).

3.4 Landsat images

In order to analyze the relationship between glacier mass balance and changes in glacier extent, two Landsat Thematic Mapper (TM) scenes, one Landsat Enhanced Thematic Mapper Plus (ETM+) scene and three Landsat Operational Land Imager (OLI) scenes were employed in this study (Table 1). It is better that Landsat images were acquired in the same year with SRTM and TerraSAR-X/TanDEM-X acquisitions, while because of the low quality of Landsat images in 2000 and 2014, Landsat TM/ETM+ images in 2001 and Landsat OLI images in 2015 with high quality were selected in this study. All Landsat images are available from the United States Geological Survey (USGS), and are orthorectified with the SRTM and ground control points from the Global Land Survey 2005 (GLS2005) dataset. Amongst the Landsat images, the co-registered TerraSAR-X coherence image, the SRTM-X DEM and Topographic Maps, almost no horizontal shift was observed. For Landsat ETM+/OLI images, pan-sharpening employing principal component analysis was performed to enhance the spatial resolution to 15 m.

4 Methods

4.1 Glacier Inventory

The outlines of glaciers in October 1980 were delineated manually from Topographic Maps. These maps were geo-referenced and rectified with a kilometer grid, and validated by reference to the original aerial photographs to update the first Chinese Glacier Inventory (Wu et al., 2016b).

Global inventory of glacier outlines can be available through the Randolph Glacier Inventory (Arendt et al., 2015). For the Kangri Karpo Mountains, these glacier outlines are taken from “the

Second Chinese Glacier Inventory" (CGI2) that delineated from Landsat TM on 8 September 2005 (Guo et al., 2015). An inventory of high-mountain Asian glaciers named "Glacier Area Mapping for Discharge from the Asian Mountains" was compiled from 356 Landsat ETM+ scenes in 226 path-row sets (Nuimura et al., 2015). The GAMDAM outlines are nearly all from 1999-2003 and thus conform with the recommendation for the compilation of glacier inventory to select imagery as close to 2000 as possible (Arendt et al., 2015; Paul et al., 2009). Hence, Landsat TM/ETM+ scenes were used to validate and update the CGI2 and GAMDAM glacier inventory, and generated the 2000 inventory of the detailed study area.

A semi-automated approach using the TM3/TM5 band ratio was applied to delineate glacier outlines in 2015 using Landsat OLI images (Bolch et al., 2010b; Paul et al., 2009; Racoviteanu et al., 2009). To ensure that ice patches were larger than 0.01 km^2, a 3 by 3 median filter was applied to eliminate isolated pixel (Bolch et al., 2010b; Wu et al., 2016b). Then, the derived glacier polygons are checked manually against images from adjacent years with less or no snow and cloud-free, to discriminate proglacial lakes, seasonal snow, boulders on the glacier and debris-covered ice (Fig. 3). The final contiguous ice coverage was divided into individual glacier polygons using topographical ridgelines (TRLs), which were automatically generated based on the SRTM-C DEM (Guo et al., 2011).

The best way to assess the accuracy of glacier outlines is to compare extracted results with independently digitized glacier outlines from high resolution aerial imagery at random locations (Bolch et al., 2010a; Paul et al., 2003). Previous studies indicated that the average offsets between glacier outlines derived from Topographic Maps and Corona-image outlines was ±6.8 m (Wu et al., 2016b), and the average offsets between Landsat-image outlines and real-time kinematic differential GPS (RTK-DGPS) measurements, Google Earth™ images with a spatial resolution better than 1 m, were ±10 m and ±30 m for the delineation of clean and debris-covered ice, respectively (Guo et al., 2015). On the basis of these average offsets, mean relative errors of ±1.3%, ±2.0% and ±2.4% were calculated for glacier area in 1980, 2000 and 2015, respectively.

4.2 Glacier Length

Glacier length is a key parameter in glacier inventory and its vector representation (glacier centerlines) is important to model future glacier evolution and calculate glacier ice volume (Le Bris and Paul, 2013). Some researchers defined it as the central flowline from the highest glacier elevation to the terminus, whereas others regard the length of the longest flowline as glacier length (Kienholz et al., 2014; Leclercq et al., 2014). The length change can be calculated by intersecting the central flowline with the respective glacier outline (Paul and Svoboda, 2010), or calculated as the average length from the intersection of the glacier outlines with the stripes which drawn parallel to the main flow direction of the glaciers (Koblet et al., 2010).

In this study, a new strategy based on a glacier axis concept from glacier morphology perspective was applied that requires only glacier outlines and a DEM as input (Yao et al., 2015). As the base for the glacier axis concept we assume that the main direction of any given glaciers can be defined as a curved line from its highest to its lowest elevation. At first, the outline of given glacier is divided into two curved lines by its highest and its lowest point. Using the two curved lines, the polygon of given glacier is divided into two regions by Euclidean distance. Glacier axis is the common boundary of the two regions, and it can be defined as the glacier centerline. An error estimation of the resulting glacier centerlines was performed that compared the semi-automatically generated results to high resolution aerial imagery at the terminus of glacier

centerlines. A Corona image with a resolution of 4 m and Google Earth™ images with a resolution better than 1 m were used to evaluate the accuracy of glacier centerlines. Hence, the uncertainties of glacier centerlines from Topographic Maps and Landsat images are no more than 6 m and 7.5 m, respectively.

4.3 Glacier elevation changes

The TerraSAR-X/TanDEM-X acquisitions were processed by differential SAR interferometry (DInSAR) (Neckel et al., 2013a) using GAMMA SAR and interferometric processing software (Werner et al., 2000).

The interferometric phase of the single-pass TerraSAR-X/TanDEM-X interferogram could be described by

$$\Delta_{\phi\mathrm{TSX/TDX}} = \Delta_{\phi\mathrm{orbit}} + \Delta_{\phi\mathrm{topo}} + \Delta_{\phi\mathrm{atm}} + \Delta_{\phi\mathrm{scat}} \quad (1)$$

where $\Delta_{\phi\mathrm{TSX/TDX}}$ is the difference of phases of phases $\phi\mathrm{TSX}$ and $\phi\mathrm{TDX}$ simultaneously acquired by TerraSAR-X and TanDEM-X. $\Delta_{\phi\mathrm{orbit}}$ is the phase difference induced by the different acquisition geometry of the SAR sensors, and $\Delta_{\phi\mathrm{topo}}$ is the phase difference induced by topography. $\Delta_{\phi\mathrm{atm}}$ and $\Delta_{\phi\mathrm{scat}}$ are the phase differences induced by atmospheric conditions and different scattering on the ground. As the data of TerraSAR-X/TanDEM-X were acquired simultaneously, the same atmospheric conditions and scattering are assumed for both SAR antennas, which set $\Delta_{\phi\mathrm{atm}}$ and $\Delta_{\phi\mathrm{scat}}$ in Eq. (1) to zero. $\Delta_{\phi\mathrm{orbit}}$ could be removed from the interferogram by subtracting a simulated flat-earth phase trend (Rosen et al., 2000).

The DInSAR approach can be described by

$$\Delta_{\phi\mathrm{diff}} = \Delta_{\phi\mathrm{TSX/TDX}} - \Delta_{\phi\mathrm{SRTM-C}} \quad (2)$$

where $\Delta_{\phi\mathrm{SRTM-C}}$ is the interferometric phase of the February 2000 SRTM-C acquisition. Due to the unavailable of the raw interferometric data of the SRTM-C acquisition, $\Delta_{\phi\mathrm{SRTM-C}}$ was simulated from SRTM-C DEM data using the satellite geometry and baseline model of the TerraSAR-X/TanDEM-X pass. Therefore the differential phase $\Delta_{\phi\mathrm{diff}}$ is solely based on changes in $\Delta_{\phi\mathrm{topo}}$ between data acquisitions (Neckel et al., 2013b).

In order to improve the phase-unwrapping procedure and minimize errors, the unfilled finished SRTM C-band DEM were employed in this study. Before generating the differential interferogram, precise horizontal offset registration and fitting between the SRTM C-band DEM and the TerraSAR-X/TanDEM-X acquisitions is necessary. Based on the relation between the map coordinates of the SRTM C-band DEM segment covering the TerraSAR-X/TanDEM-X master file, and the SAR geometry of the respective master file, an initial lookup table was calculated. While the areas of radar shadows and layover in the TerraSAR-X/TanDEM-X interferogram would induce gaps in the lookup table, a method of linear interpolation between the gap edges in each line of the lookup table was used to fill these gaps. The offsets between the master scene and the simulated intensity of the SRTM C-band DEM, were calculated using cross correlation optimization of the simulated SAR images employing *GAMMA's offset_pwrm* module. The horizontal registration and geocoding lookup table were refined by these offsets. The SRTM C-band DEM was translated from geographic coordinates into SAR coordinates via the refined geocoding lookup table, and conversely, the final difference map was translated from SAR coordinates into geographic coordinates. Then a differential interferogram was generated by the TerraSAR-X/TanDEM-X interferogram and the simulated phase of the co-registered SRTM C-band DEM. An adaptive filtering approach was used to filter the differential interferogram (Goldstein and Werner, 1998), and then *GAMMA's* minimum cost flow (MCF) algorithm was

employed to unwrap the flattened differential interferogram. According to the computed phase-to-height sensitivity and select ground control points (GCPs) from the respective off-glacier pixel locations in the SRTM C-band DEM, the unwrapped differential phase was converted to absolute differential heights. While, a residual not covered by the baseline refinement would be existed, and can be regarded as a linear trend that estimated by a two dimensional first order polynomial fit in off-glacier regions. The linear trend and a constant vertical offset were removed from the maps of absolute differential heights. Finally, the resulting data sets were translated to a metric cartographic coordinate system with 30 m × 30 m pixel spacing (Neckel et al., 2013a). The same method of DInSAR was employed to acquire the glacier elevation change from 1980 to 2014 with the data sets of TOPO DEM and TerraSAR-X/TanDEM-X acquisitions.

For the glacier elevation change from 1980 to 1999, a difference map was constructed by common DEM differencing with TOPO DEM and SRTM C-band DEM (Bolch et al., 2011; Nuth and Kääb, 2011; Pieczonka et al., 2013; Wei et al., 2015a). Relative horizontal and vertical distortions between the two data sets, can be corrected by statistical approaches that based on the relationship between elevation difference and slope, aspect (Nuth and Kääb, 2011). Elevation differences in off-glacier regions were used to analyze the consistency of TOPO DEM and SRTM C-band DEM (Fig. 4). Outliers of elevation differences, usually around data gaps and near DEM edges, were omitted with values exceeding ±100 m (Berthier et al., 2010; Bolch et al., 2011). The vertical biases and horizontal displacements could be adjusted simultaneously using the substantial cosinusoidal relationship between standardized vertical bias and topographical parameters (slope and aspect). And the biases that caused by different spatial resolutions between DEMs, could be adjusted by the relationship between elevation differences and maximum curvatures (Gardelle et al., 2012a; Nuth and Kääb, 2011).

The penetration depth of SRTM C-band radar beam into snow and ice need to be considered for elevation changes of glacier surfaces (Berthier et al., 2006; Gardelle et al., 2012a; Pieczonka et al., 2013). Penetration depth can range from 0 to 10 m depending on a variety of parameters such as snow temperature, density and water content (Berthier et al., 2006; Dall et al., 2001). As a first approximation, the penetration depth of SRTM X-band radar beam is much smaller than C-band, the elevation difference between these two data sets can be considered as the penetration of SRTM C-band radar beam into snow and ice (Gardelle et al., 2012a). The elevation differences between SRTM C-band and X-band indicate that the penetration depth of the C-band averaged 1.24 m in the study area. The mean value of the SRTM C-band penetration over glaciers in Kangri Karpo Mountains is in agreement with Gardelle et al. (2013), who found penetration of 1.7 m in eastern Nyainqentanglha Mountains (named Hengduan Shan in Gardelle et al. (2013)).

4.4 Mass balance and error estimation

In order to convert the derived surface elevation changes into the mass balance of glaciers, a density of ice/firn/snow should be considered. A value of 900 kg m^{-3} was applied to assess the mass changes in water equivalent (w.e.) from elevation differences, and then adding an ice density uncertainty of 17 kg m^{-3} (Gardner et al., 2013; Neckel et al., 2013b) .

For the accuracy assessment of TOPO DEM and SRTM C-band DEM, the elevation product of Geoscience Laser Altimeter System (GLAS) carried on-board the Ice Cloud and Elevation Satellite (ICESat) was utilized in this study (Neckel et al., 2013a). All available GLAS elevation data for the study area were obtained from the National Snow and Ice Data Center (NSIDC) (release 634; product GLA 14). Because of the effect of clouds during the time of data acquisition,

some GLAS elevation data cannot represent the true altitude of ground surface. Outliers of elevation difference between GLA 14 and multi-source of DEMs in off-glacier regions were removed from the analysis with values exceeding ±100 m. Compared to the GLAS elevation data, a mean and standard deviation of 2.74 ± 1.73 m and 2.65 ± 1.48 m for TOPO DEM and SRTM C-band DEM, respectively. Due to the GCPs that convert the unwrapped TerraSAR-X/TanDEM-X interferogram into absolute heights was selected from the respective off-glacier pixel locations in the SRTM C-band DEM, vertical bias of TerraSAR-X/TanDEM-X DEM and GLA 14 is similar with the bias of SRTM C-band DEM and GLA 14.

For an error estimate of the derived surface elevation changes, the residual elevation differences were estimated in off-glacier regions assuming that these areas did not change in height between 1980 and 2014 and that elevations should be equal in TOPO DEM, SRTM C-band DEM and TerraSAR-X/TanDEM-X DEM. The mean elevation difference (MED) over off-glacier regions between the final difference maps was in the range of -1.42 to 0.75 m (Table 2). Because averaging over larger regions reduces the errors, the standard deviation (STDV) over off-glacier regions would probably overestimate the uncertainty for larger samples. Thus, the uncertainty can be estimated by the standard error of the mean (SE):

$$SE = \frac{STDV}{\sqrt{N}} \quad (3)$$

where N is the number of the included pixels. To avoid the effect of autocorrelation, de-correlation length of 600 m and 200 m was employed for difference maps that derived by common DEM differencing and DInSAR (Bolch et al., 2011; Neckel et al., 2013a). Then, the overall errors of the derived surface elevation changes can be estimated using SE and MED over off-glacier regions:

$$\sigma = \sqrt{\mathrm{MED}^2 + \mathrm{SE}^2} \quad (4)$$

Finally, the root of sum of squares of the estimated errors of glacier area and surface elevation changes, and ice density uncertainty of 17 kg m^{-3}, were used to estimate the overall errors of mass balance (Neckel et al., 2013a).

5 Results

5.1 Area change

According to the 2015 inventory, the Kangri Karpo Mountains contain 1166 glaciers, with an area of 2048.50 ± 48.65 km^2, and the mean glacier size is 1.76 ± 0.04 km^2 (Fig. 5). The highest number of glaciers can be found in the size class 0.1-0.5 km^2, whereas glaciers between 1-5 km^2 cover the largest area (Fig. 5A). Only two glaciers area larger than 50 km^2, the largest glacier is Yalong Glacier and another is Xirinongpu Glacier, with glacier area of 173.00 ± 0.67 km^2 and 90.28 ± 0.23 km^2, respectively. Glaciers area in Kangri Karpo Mountains present a normal hypsometry, about 76.9% of glacier area lies in the 4500-5500 m elevation range. Azha Glacier is the glacier with the lowest glacier tongue position, and the elevation of glacier tongue at 2551 m (Fig. 5B). Median elevation of the glaciers in Kangri Karpo Mountains is situated at around 4852 m, 5215 m for glaciers on the north slope and 4639 m on the south. This is consistent with the tendency of equilibrium line altitude in southeast Tibetan Plateau (Su et al., 2014). The mean glacier surface slope in the Kangri Karpo Mountains is 24.1 º, with most in the 12-32 ºrange that accounts for 80.5% of the glaciers and 85.4% of their area. Most glaciers have a SE, S or SW aspects, account for 59.2% and 80.9% of glacier number and area, respectively.

Comparing the total area of all glaciers in 1980 with that in 2015, ice cover in the Kangri Karpo Mountains diminished by 679.51 ± 59.49 km^2 (24.9% ± 2.2%) or 0.71% ± 0.06% a^{-1}. Small glaciers shrunk in area in larger percentage (Fig. 5C). Meanwhile, absolute area loss was higher for larger glaciers. Analysis of the glacier hypsography indicated that ice coverage disappeared completely below 2500 m, the highest absolute area loss occurred in the 4500-4700 m a.s.l. altitude range, and ice coverage remains almost unchanged above 5800 m. The average minimum elevation of the glaciers increased by 106 m, while median elevation rose about 56 m from 4796 to 4852 m.

There was a slight tendency that the rate of glaciers shrinkage from 1980 – 2000 was lower than those from 2000 – 2015 in the detailed study area of Kangri Karpo Mountains (Table 3). In the period of 1980 – 2000, glacier area decreased by 63.72 ± 9.06 km^2 from its original 784.60 km^2 (8.1% ±1.2%) or 0.41% ± 0.06% a^{-1}. Between 2000 and 2015, glaciers experienced a reduction of 56.00 ± 10.97 km^2 (7.8% ± 1.5%) or 0.52% ± 0.10% a^{-1}. A detailed analysis of ten sample glaciers confirmed that all glaciers decreased continuously throughout all investigated periods (Table 4). Percentage area loss varied between 8.6% (WGI ID/GLIMS ID: 5O291B0200/G097005E29155N, the smallest glacier area loss) and 20.9% (Parlung No. 10 Glacier, the largest glacier area loss) from 1980 – 2015. The largest loss of absolute area reached 20.43 km^2 for Yalong Glacier, and lowest reached 1.04 km^2 for Parlung No. 10 Glacier.

5.2 Length change

Comparing the termini of all glaciers, only nine glaciers advanced while others retreated in the Kangri Karpo Mountains from 1980 – 2015. The nine glaciers experienced a mean advance of 14.8 m a^{-1}, and the length of centerlines increased between 103 m and 1547 m. The terminus elevation decrease of these advanced glaciers averaged at 191 m, varying between 34 m (the smallest lowering from 4796 m to 4762 m a.s.l. altitude) and 412 m (the largest one from 4362 m to 3949 m a.s.l. altitude) (Table 5). Based on different glacier size, slope and aspect, 86 glaciers were selected from all retreated glaciers to analyze the changes of length. These selected glaciers experienced a mean recession of 759 m (21.7 m a^{-1}) with smallest of 6 m and largest of 3956 m.

Similar to area change of the glaciers in the case study region, these glaciers have shown accelerated retreat during the two periods from 1980 – 2000 and from 2000 – 2015 as measured in glacier length (Table 6). Glaciers experienced a mean length reduction of 21.0 m a^{-1} (varying from 2.5 m a^{-1} to 104.2 m a^{-1}) in the period of 1980 – 2000 and 22.6 m a^{-1} from 2000 – 2015 (varied between 1.3 m a^{-1} and 144.8 m a^{-1}). The recession of Yalong Glacier changed from 78.0 m a^{-1} in 1980 – 2000 to 13.6 m a^{-1} in 2000 – 2014, while the average rates of retreat increased significantly for Azha Glacier in the two sub-periods of 1980 – 2000 and 2000 – 2015, with a mean recession of 11.3 m a^{-1} and 144.8 m a^{-1}, respectively.

5.3 Mass balance

The average elevation change of the entire glacier surfaces in the case study area of Kangri Karpo Mountains was -17.46 ± 0.54 m from 1980 – 2014. The glaciers, with an area of 788.28 km^2, have experienced a mean thinning of 0.51 ± 0.09 m a^{-1}, or mean mass loss of 0.46 ± 0.08 m w.e. a^{-1}, equivalent to an overall mass change of -13.76 ± 0.43 Gt for the case study area during 1980 – 2014. Thinning of these glaciers has speeded up during the periods of 1980-2000 and 2000 – 2014. From 1980 – 2000, glaciers have thinned by 5.30 ± 0.77 m on average, and experienced a mass loss of 0.24 ± 0.16 m w.e. a^{-1}. Then a surface lowering of 11.04 ± 0.43 m was found from 2000 –

2014, with a mass loss of 0.71 ± 0.10 m w.e. a^{-1} (Fig. 6 and Table 7).

Heterogeneous glacier mass balance was presented in the detailed study area of Kangri Karpo Mountains during 1980 – 2014. Glaciers, with an area of 471.05 ± 3.03 km^2 in the drainage basin of 5O282B, experienced greater mass deficit of 0.51 ± 0.22 m w.e. a^{-1} from 1980 – 2014, and mean mass deficit of 0.30 ± 0.14 m w.e. a^{-1} and 0.76 ± 0.22 m w.e. a^{-1} during the periods of 1980 – 2000 and 2000 – 2014, respectively. Mean mass deficit of 0.39 ± 0.11 m w.e. a^{-1} in the drainage basin of 5O291B was smaller than those in 5O282B drainage basin during 1980 – 2014. Glaciers with an area of 317.22 ± 4.27 km^2 in 5O291B drainage basin experienced accelerating mass deficit during the periods of 1980 – 2000 and 2000 – 2014, with mean mass deficit of 0.13 ± 0.16 m w.e. a^{-1} and 0.63 ± 0.04 m w.e. a^{-1}.

Prominent thickening (elevation increase) was found on the termini of two glaciers on the southern slope of the Kangri Karpo Mountains (Fig. 6C, WGI: 5O291B0113 and 5O291B0117). There have 3.79 km^2 and 3.70 km^2 debris-covered areas on the two glaciers, account for 20.6% and 31.4% of individual glacier areas, respectively. Meanwhile, the lengths of debris-covered regions account for 69.4% and 63.3% of individual glacier lengths. Probably the effect of debris cover, the glacier termini of 5O291B0113 and 5O291B0117 remain stable between October 1980 and October 2015.

6 Discussion

6.1 Uncertainty

The uncertainty of glacier outlines was caused by positional and processing errors associated with glacier delineation (Bolch et al., 2010a; Racoviteanu et al., 2009). Seasonal snow, cloud and debris cover complicated glacier mapping precisely (Paul et al., 2013). The accuracy of glacier outlines in this study was estimated by compare extracted results with independently digitized glacier outlines from high resolution aerial imagery at random locations. An uncertainty model was employed to assess accuracy estimated in this study (Pfeffer et al., 2014). The delineation uncertainty of glaciers in the Kangri Karpo Mountains in 2015 was about 24.33 km^2 using the uncertainty model, that is smaller than the uncertainty of 48.65 km^2 in this study. Main reason for this discrepancy is probably that the delineation uncertainty of glaciers have been overestimated in this study, especially in the area of debris-covered ice and exposed bedrock that surrounded by ice cover.

For the uncertainty of mass balance, the penetration depth of SRTM C-band radar beam into snow and ice was critical issue when SRTM DEM was employed for geodetic mass balance calculations. The penetration depth of SRTM C-band radar beam can be estimated by comparing the SRTM C-band with the SRTM X-band DEM (Gardelle et al., 2012a; Käab et al., 2012). Previous studies indicated that the penetration depth decreases as temperature and water content of surface snow cover rise (Surdyk, 2002), and penetration depths at 10 GHz from 2.1 m to 4.7 m were measured in Antarctica (Davis and Poznyak, 1993). Glaciers in eastern Nyainqentanglha Mountains are predominantly monsoonal influenced and have more snow moisture and higher temperatures than the Antarctic ice sheet (Shi and Liu, 2000). Hence, the penetration correction is suitable under the assumption that the influence of slight penetration of the X-band is negligible. The mean SRTM C-band penetration was 1.24 m in Kangri Karpo Mountains, led to mass changes on average of +0.06 m w.e. a^{-1} and -0.08 m w.e. a^{-1} for the periods of 1980 – 2000 and 2000 – 2014.

Another issue is the lack of information in several regions due to data voids in accumulation area. Different suitable assumptions or elevation changes in the accumulation regions were used to fill the data voids and to assess the impact on mass balance (Pieczonka et al., 2013; Shangguan et al., 2015). In this study, the information of elevation change exists in all altitudinal zones from 2400 m to 6600 m a.s.l., and the area of data voids was too small (0.7% above 6000 m a.s.l. in area) to affect the mass balance significantly. Hence, data voids can be neglected when mass balance was estimated by all glaciers area in the detailed study area, average surface elevation change and ice density.

6.2 Glacier change of area and length

This study found ice cover in the Kangri Karpo Mountains diminished between 1980 and 2014 of about 0.71% ±0.06% a^{-1}. In the period of 1980 – 2000, glacier area decreased by 0.41% ± 0.06% a^{-1} in the case study area, and then this value increased to 0.52% ±0.10% a^{-1} after 2000. Our result is in agreement with previous study, that found shrinkage of 0.57% a^{-1} in the southeastern Tibetan Plateau from 1980-2001 (Yao et al., 2012a). The shrinkage rate of previous study is larger than our result slightly, main reason for that is probably the difference of glacier size. The mean glacier sizes are about 2.07 km^2 and 6.54 km^2 in the Kangri Karpo Mountains and in the detailed study area in 1980, and greater relative loss for smaller glaciers was found in this study and previous studies (Wei et al., 2014; Wu et al., 2016b).

Compared with the retreat of mountain glaciers in the western China, glaciers in Kangri Karpo Mountains have experienced extremely strong glacial retreat. The glacier retreat of about 0.71% a^{-1} is lower than that in Altay Mountains (0.75% a^{-1}) (Yao et al., 2012b), but larger than that in other regions of western China, such as Tian Shan Mountains (0.22% a^{-1}) (Wang et al., 2011), eastern Pamir (0.25% a^{-1}) (Zhang et al., 2016b), wester Kunlun Mountains (0.09% a^{-1}) (Bao et al., 2015), Qilian Mountains (0.47% a^{-1}) (Sun et al., 2015), Tibetan Plateau interior area (0.26% a^{-1}) (Wei et al., 2014).

The location of glacier terminal is often measured by remote sensing and investigation in the field. Due to the differences in the periods studied and spatial scales, the length changes of glacier centerlines in this study are slower than previous studies, except for Azha Glacier (Liu et al., 2006; Yang et al., 2010; Yao et al., 2012a). The investigation of terminus variation on Parlung No. 10 Glacier was surveyed from 2006 – 2008, the period of survey is too short to represent length change of glacier centerlines over long periods of time (Yang et al., 2010). Compared the length change of Azha Glacier in different periods, -56.1 m a^{-1} from 1973 – 2005 (Yao et al., 2012a), -65 m a^{-1} from 1980 – 2006 (Yang et al., 2010) and -70 m a^{-1} from 1980 – 2015 (this study), we can found that Azha Glacier have experienced greater retreat after 2000s than that before 2000s. The length change of Yalong Glacier from 1980 – 2000 in this study is similar with Liu et al. (2006), who found retreat of 73 m a^{-1} of Yalong Glacier between 1980 and 2001. And then the average rate of retreat decreased significantly for Yalong Glacier after 2000.

For advanced glaciers, the mean glacier size is about 0.51 km^2 and mean glacier surface slope is about 27.9 °, most glaciers have an S or SW aspect, and mean accumulation area ratio (AAR) is 51. Previous studies also found advanced glaciers in Kangri Karpo Mountains (Liu et al., 2006; Shi et al., 2006). Compared with the CGI2 and GAMDAM glacier inventory, the location of most glacier termini in 2000 are very close to that in 2014, indicated that glacier advanced mainly occurs before 2000. Due to the special geographic location and climate feature, the qualities of Landsat MSS/TM images are too low to identify glacier termini. Fortunately, two Landsat TM

scenes (LT51340401994189BKT00 and LT51340401988301BJC00) with high quality can be employed in this study. Compared the glacier termini that acquired from Landsat scenes, such as Glacier 5O282B0111 (Fig. 3B), glacier advanced mainly occurs before 1988, and glacier retreated continuously after that (Fig. 7). Main reason for this phenomenon is probably that the increase of high precipitation (Shi et al., 2006). Annual precipitation dataset from 1980 to 2012, collected from the three nearest meteorological stations (Bomi, Zuogong and Zayu), indicated that maximum precipitation (1153 mm in 1988) is 1.6 times the minimum precipitation (714 mm in 1981) at Bomi (29°52′N, 95°46′E, 2736 m a.s.l.), maximum precipitation (683 mm in 1987) is 2.3 times the minimum precipitation (302 mm in 1983) at Zuogong (29°40′N, 97°50′E, 3780 m a.s.l.), and maximum precipitation (1091 mm in 1988) is 1.7 times the minimum precipitation (624 mm in 1982) at Zayu (28°39′N, 97°28′E, 2423 m a.s.l.). Supposing that the precipitation fluctuation in high elevation glacier area had been consistent with that at the three nearest meteorological stations, the change of precipitation or glacier accumulation certainly have significant influence on terminus fluctuation of glaciers. Due to the complicated terrains, the accumulation of glaciers varies greatly, and the response of glacier movement is not quite the same, individual glaciers advanced during 1980 – 1988.

6.3 Glacier thinning and mass balance

A comparison of glacier thickness changes show that significant differences are found over eastern Nyainqentanglha Mountains. Using SRTM DEM and SPOT5 DEM (24 November 2011), glaciers experienced a mean thinning of 0.39 ± 0.16 m a^{-1} in eastern Nyainqentanglha Mountains (named Hengduan Shan) (Gardelle et al., 2013). Based on ICESat and SRTM, Kääb et al. (2015), Neckel et al. (2014) and Gardner et al. (2013) acquired different results over the Kangri Karpo Mountains, with glacier thickness loss of 1.34 ± 0.29 m a^{-1}, 0.81 ± 0.32 m a^{-1} and 0.30 ± 0.13 m a^{-1} during 2003 to 2009, respectively. Using SRTM DEM and TerraSAR-X/TanDEM-X acquisitions (18 February 2014 and 13 March 2014), glaciers experienced a mean thinning of 0.79 ± 0.11 m a^{-1} in Kangri Karpo Mountains. At a first glance, the result of glacier thickness loss in this study is in agreement with Neckel et al. (2014), and has significant differences with Kääb et al. (2015). Main reason for this discrepancy is the different estimation of SRTM C-band penetration. An average SRTM C-band penetration of 1.24 m was used for Kangri Karpo Mountains that estimated from the difference of SRTM C-band and X-band DEMs (Gardelle et al., 2012a). While an average penetration of 8-10 m (7-9 m if based on the winter trends that might alternatively be assumed to reflect February conditions) was employed for eastern Nyainqentanglha Mountains (Kääb et al., 2015). Previous studies indicated that the penetration depth varies with temperature and water content (Surdyk, 2002), and penetration depths of SRTM C-band from 1.4 m to 3.4 m were estimated over the Pamir-Karakoram-Himalaya (Gardelle et al., 2013; Kääb et al., 2012). The characteristics of glaciers in eastern Nyainqentanglha Mountains are similar with that in eastern Himalaya (Shi et al., 2008b). Therefore, the penetration in this study is more suitable under the assumption that the penetrations in eastern Nyainqentanglha Mountains and eastern Himalaya are similar.

Field measurement of mass balance is the best indicator of glacier change. A monitoring program has been carried out on Parlung No. 4 Glacier (5O282B0004/G096920E29228N) and Parlung No. 10 Glacier (5O282B0010/G096904E29286N), both located on the northern slope of the Kangri Karpo Mountains. Large ice deficit were found on the two monitored glaciers at rates of -0.71 m w.e. a^{-1} from May 2006 to May 2007 and -0.78 m w.e. a^{-1} during 2005 – 2009,

respectively (Yang et al., 2008; Yao et al., 2012a). Based on SRTM DEM and TerraSAR-X/TanDEM-X acquisitions (18 February 2014), the two glaciers experienced large surface lowering from 2000 to 2014, with mean mass deficit of 0.65 ± 0.22 m w.e. a^{-1} and 0.67 ± 0.22 m w.e. a^{-1}. The comparison between filed measurements of mass balance and the result of this study indicated that there was high consistency of glacier mass deficit about Parlung No. 4 Glacier and Parlung No. 10 Glacier.

Interestingly is the bigger thinning on the debris-covered region of -0.99 ± 0.09 m a^{-1} on average than clean-ice region of -0.89 ± 0.08 m w.e. a^{-1} in the 2800 – 5300 m a.s.l. altitude range from 1980 – 2014 (Fig. 8). 2800 m a.s.l. was the lowest altitude of clean-ice region and 5300 m a.s.l. was the highest altitude of debris-covered region. Due to complex surface conditions, such as supraglacial lakes, ice cliffs and heterogeneity of debris cover, the mass loss patterns on the debris-covered tongue are complicated (Pellicciotti et al., 2015). It is generally believed that ice ablation rate is highly reduced with the thick debris-cover due to the insulation effect of debris. However, previous studies found that glacier ablation on debris-covered regions were greater than on the exposed ice regions, when debris thickness is less than critical thickness (Nakawo and Young, 1981; Pu et al., 2003; Ye et al., 2015; Zhang et al., 2011; Zhang et al., 2016a). The location of debris-covered regions, in the lower altitudes with higher temperature, and the development of supraglacial lakes and ice cliffs are probably the reasons for the larger mass loss on the debris-covered regions (Benn et al., 2012; Sakai and Fujita, 2010).

Overall, negative elevation changes were found in glacier tongue regions except for two glaciers in the southern slope of the Kangri Karpo Mountains (Fig. 6C). Compared the average elevation changes of the two glaciers tongue surface during 1980-2000 and 2000-2014, positive elevation changes were found between October 1980 and February 2000, and negative elevation changes were found after 2000. The two glaciers showed positive elevation changes at the termini, while elevation changes are unknown in accumulation area of the two glaciers due to data voids. This phenomenon could be interpreted as glacier surging (Cuffey and Paterson, 2010), or result from the increase of high precipitation (Shi et al., 2006).

6.4 Climatic considerations

The climate in Kangri Karpo Mountains is characterized be the westerly in winter and the Indian monsoon in summer (Li et al., 1986). While the effects of westerly are weak in the study area due to the block of Tibetan Plateau. Hence, the accumulation on glaciers in Kangri Karpo Mountains is supplied by summer monsoon precipitation (Bolch et al., 2010a; Yao et al., 2012a). Previous studies indicated that the Tibetan Plateau has experienced an overall surface air warming since the mid-1950s (Duan et al., 2015; Li et al., 2010; Liu et al., 2008; Liu et al., 2009; Qin et al., 2009; Yang et al., 2014; Yao et al., 2012a; You et al., 2010). Different trend of average annual temperature results from different data in the southeastern TP. Based on temperature data from meteorological stations, the southeastern TP present the lowest warming rate (Duan et al., 2015), while the most warming rate was found from the MODIS land surface temperature (MODIS LST) in the southeastern TP (Yang et al., 2014), even decreasing trend of average annual temperature was found from the National Centers for Environmental Prediction/National Center for Atmospheric Research (NCEP/NCAR) Reanalysis data (You et al., 2010). The changes in air temperature were accompanied by the changes in precipitation due to variations in monsoonal activity. Based on the Global Precipitation Climatology Project (GPCP) data, precipitation decreased in the southeastern TP from 1979 to 2010 (Yao et al., 2012a). While positive trend of

annual precipitation was found from Chinese meteorological stations data in the southeastern TP, precipitation amount increased and the frequency of severely dry events decreased significantly (Li et al., 2010). Due to the ambiguous of climate change, the presented glacier changes and mass balance cannot be explained by the above summarized climate variations directly.

In order to analyze the response of glaciers to climate change, air temperature and precipitation datasets were collected from the China Meteorological Forcing Dataset (CMFD, 1979.01.01 – 2012.12.31) (Chen et al., 2011; He and Yang, 2011), which produced by merging a variety of data sources, including meteorological station data, TRMM satellite precipitation analysis data, GEWEX-SRB downward shortwave radiation data and GLDAS data (http://westdc.westgis.ac.cn/data/7a35329c-c53f-4267-aa07-e0037d913a21). The horizontal distributions of surface temperature change and precipitation change from May to September derived from the CMFD data was shown in Fig. 9. It is clear that warming is a dominant phenomenon in the southeastern TP during recent decades. The warming rate on the northern slope of the Kangri Karpo Mountains is larger than that on the southern slope slightly. The law of precipitation change was inconsistent that an increasing trend was present in much of Kangri Karpo Mountains, but a decreasing trend in the eastern Kangri Karpo Mountains. The changes of air temperature and precipitation are confirmed by three nearest meteorological stations datasets, which is Bomi (2736 m a.s.l.), Zuogong (3780 m a.s.l.) and Zayu (2423 m a.s.l.) (Liu et al., 2006; Yang et al., 2010). The air temperature at the three meteorological stations increased slightly from 1980-2000, and then it increased significantly after 2000. Despite large inter-annual fluctuation of precipitation, statistically significant trends are not evident at the three stations (Wu et al., 2016a; Yang et al., 2010).

For the rainfall-variation law, a slightly increasing trend was present in the detailed study area of Kangri Karpo Mountains during 1980 – 2012. The increase of precipitation results in more glacier accumulation, while glaciers have experienced an intense mass deficit in the detailed study area of Kangri Karpo Mountains. It can be concluded that other factors are playing a more important role in glacier mass deficit. For the change of temperature, warming was present in the detailed study area of Kangri Karpo Mountains during 1980 – 2012. And the warming rate on the northern slope of the Kangri Karpo Mountains is larger than that on the southern slope slightly. A small warming rate was present from 1980 – 2000, and increased to large warming rate thereafter. This is consistent with the tendency of glaciers change. Glaciers have experienced an intense area reduction and mass deficit in the Kangri Karpo Mountains, and mean mass deficit in the drainage basin of 5O282B (located on the northern slope of detailed study area) was larger than that in the drainage basin of 5O291B (located on the southern slope of detailed study area) during 1980 – 2014. Meanwhile, the rate of glaciers shrinkage and mass loss from 1980 – 2000 were lower than those from 2000 – 2015. Hence, glaciers change in the Kangri Karpo Mountains can be attributed to climate warming.

7 Conslusions

This study estimated glacier area, glacier length, surface elevation and mass balance of the Kangri Karpo Mountains for the period of 1980 – 2015 based on Topographic Maps, Landsat images, SRTM and TerraSAR-X/TanDEM-X acquisitions.

Our results show that the Kangri Karpo Mountains contain 1166 glaciers, with an area of 2048.50 ± 48.65 km^2 in 2015. Ice cover in the Kangri Karpo Mountains diminished by 679.51 ± 59.49 km^2 (24.9% ± 2.2%) or 0.71% ± 0.06% a^{-1} from 1980 – 2015. Comparing the terminal of all

glaciers, only nine glaciers advanced while others retreated in the Kangri Karpo Mountains from 1980 – 2015. Compared with the retreat of mountain glaciers in the western China, glaciers in Kangri Karpo Mountains have experienced extremely strong glacial retreat.

The average elevation change of the entire glacier surfaces in the detailed study area of Kangri Karpo Mountains was -0.51 ± 0.09 m a^{-1}, or mean mass deficit of 0.46 ± 0.08 m w.e. a^{-1} from 1980-2014. Heterogeneous glacier mass balance was presented in the Kangri Karpo Mountains during 1980-2014. The comparison between filed measurements of mass balance and the result of this study indicated that there was high consistency of glacier mass loss about Parlung No. 4 Glacier and Parlung No. 10 Glacier. Geodetic mass balance measurements in the detailed study area of Kangri Karpo Mountains revealed that the debris-covered regions exhibit higher thinning rates than the clean-ice region on average obviously, with an average of -0.99 ± 0.09 m a^{-1} (-0.89 ± 0.08 m w.e. a^{-1}) from 1980 – 2014. There was a slight tendency that the rate of glaciers shrinkage and mass loss from 1980 – 2000 were lower than those from 2000 – 2015 in the detailed study area of Kangri Karpo Mountains.

Acknowledgements. This work was supported by the fundamental program from the Ministry of Science and Technology of China (MOST) (Grant No. 2013FY111400), the National Natural Science Foundation of China (Grant No. 41190084) and the International Partnership Program of Chinese Academy of Sciences (Grant No. 131C11KYSB20160061). Landsat images are from the U. S. Geological Survey and NASA. The GAMDAM glacier inventory is from Dr. A. Sakai . The first and second glacier inventories were provided by an immediate past MOST project (2006FY110200). The China Meteorological Forcing Dataset (CMFD) is from Cold and Arid Regions Science Data Center at Lanzhou. All SAR processing was done with the GAMMA SAR and interferometric processing software.

References

Arendt, A., Bliss, A., Bolch, T., Cogley, J. G., and Gardner, A. S.: Randolph Glacier Inventory - A dataset of global glacier outlines: Version 5.0. University of Colorado, National Snow and Ice Data Center (NSIDC), Global Land Ice Measurements from Space (GLIMS), Boulder, CO, USA. Available online at: http://www.glims.org/RGI/00_rgi50_TechnicalNote.pdf, 2015.

Bao, W., Liu, S., Wei, J., and Guo, W.: Glacier changes during the past 40 years in the West Kunlun Shan, Journal of Mountain Science, 12, 344-357, 2015.

Benn, D. I., Bolch, T., Hands, K., Gulley, J., Luckman, A., Nicholson, L. I., Quincey, D., Thompson, S., Toumi, R., and Wiseman, S.: Response of debris-covered glaciers in the Mount Everest region to recent warming, and implications for outburst flood hazards, Earth-Science Reviews, 114, 156-174, 2012.

Berthier, E., Arnaud, Y., Vincent, C., and Remy, F.: Biases of SRTM in high - mountain areas: Implications for the monitoring of glacier volume changes, Geophysical Research Letters, 33, 2006.

Berthier, E., Schiefer, E., Clarke, G. K., Menounos, B., and Rémy, F.: Contribution of Alaskan glaciers to sea-level rise derived from satellite imagery, Nature Geoscience, 3, 92-95, 2010.

Bolch, T., Menounos, B., and Wheate, R.: Landsat-based inventory of glaciers in western Canada,

1985–2005, Remote Sensing of Environment, 114, 127-137, 2010a.
Bolch, T., Pieczonka, T., and Benn, D.: Multi-decadal mass loss of glaciers in the Everest area (Nepal Himalaya) derived from stereo imagery, The Cryosphere, 5, 349-358, 2011.
Bolch, T., Yao, T., Kang, S., Buchroithner, M., Scherer, D., Maussion, F., Huintjes, E., and Schneider, C.: A glacier inventory for the western Nyainqentanglha Range and the Nam Co Basin, Tibet, and glacier changes 1976–2009, The Cryosphere, 4, 419-433, 2010b.
Chen, Y., Yang, K., He, J., Qin, J., Shi, J., Du, J., and He, Q.: Improving land surface temperature modeling for dry land of China, Journal of Geophysical Research Atmospheres, 116, 999-1010, 2011.
Cuffey, K. M. and Paterson, W. S. B.: The Physics of Glaciers (Fourth Edition), Butterworth-Heinemann/Elsevier, Burlington, MA, USA and Oxford, UK, 2010.
Dall, J., Madsen, S. N., Keller, K., and Forsberg, R.: Topography and penetration of the Greenland ice sheet measured with airborne SAR interferometry, Geophysical Research Letters, 28, 1703-1706, 2001.
Davis, C. H. and Poznyak, V. I.: The depth of penetration in Antarctic firn at 10 GHz, IEEE Transactions on Geoscience & Remote Sensing, 31, 1107-1111, 1993.
Duan, J., Li, L., and Fang, Y.: Seasonal spatial heterogeneity of warming rates on the Tibetan Plateau over the past 30 years, Scientific Reports, 5, 2015.
Farr, T. G., Rosen, P. A., Caro, E., Crippen, R., Duren, R., Hensley, S., Kobrick, M., Paller, M., Rodriguez, E., Roth, L., Seal, D., Shaffer, S., Shimada, J., Umland, J., Werner, M., Oskin, M., Burbank, D., and Alsdorf, D.: The shuttle radar topography mission, Reviews of geophysics, 45, 2007.
Gardelle, J., Berthier, E., and Arnaud, Y.: Impact of resolution and radar penetration on glacier elevation changes computed from DEM differencing, Journal of Glaciology, 58, 419-422, 2012a.
Gardelle, J., Berthier, E., and Arnaud, Y.: Slight mass gain of Karakoram glaciers in the early twenty-first century, Nature geoscience, 5, 322-325, 2012b.
Gardelle, J., Berthier, E., Arnaud, Y., and Kaab, A.: Region-wide glacier mass balances over the Pamir-Karakoram-Himalaya during 1999-2011, Cryosphere, 7, 1885-1886, 2013.
Gardner, A. S., Moholdt, G., Cogley, J. G., Wouters, B., Arendt, A. A., Wahr, J., Berthier, E., Hock, R., Pfeffer, W. T., and Kaser, G.: A reconciled estimate of glacier contributions to sea level rise: 2003 to 2009, Science, 340, 852-857, 2013.
GB/T12343.1: Compilation specifications for national fundamental scale maps —Part 1: compilation soecifications for 1:25000/1:50000/1:100000 topographic maps., General Administration of Quality Supervision, Inspection and Quarantine, Beijing, 2008.
Goldstein, R. M. and Werner, C. L.: Radar interferogram filtering for geophysical applications, Geophysical Research Letters, 25, 4035-4038, 1998.
Guo, W., Liu, S., Xu, J., Wu, L., Shangguan, D., Yao, X., Wei, J., Bao, W., Yu, P., and Liu, Q.: The second Chinese glacier inventory: data, methods and results, Journal of Glaciology, 61, 357-372, 2015.
Guo, W., Liu, S., Yu, P., and Xu, J.: Automatic extraction of ridgelines using on drainage boundaries and aspect difference, Science of Surveying and Mapping, 36, 210-213, 2011.
He, J. and Yang, K.: China Meteorological Forcing Dataset. Center, C. a. A. R. S. D., Lanzhou, 2011.
Immerzeel, W. W., Van Beek, L. P., and Bierkens, M. F.: Climate change will affect the Asian water towers, Science, 328, 1382-1385, 2010.
IPCC: Summary for policymakers. In: Climate change 2013: The physical science basis. Contribution of Working Group I to the Fifth Assessment Report of the Intergovernmental Panel on Climate Change. , Cambridge University Press Cambridge, UK and New York, NY, USA, 2013.
Käab, A., Berthier, E., Nuth, C., Gardelle, J., and Arnaud, Y.: Contrasting patterns of early

twenty-first-century glacier mass change in the Himalayas, Nature, 488, 495-498, 2012.
Kääb, A., Treichler, D., Nuth, C., and Berthier, E.: Brief Communication: Contending estimates of 2003–2008 glacier mass balance over the Pamir–Karakoram–Himalaya, The Cryosphere, 9, 557-564, 2015.
Kienholz, C., Rich, J., Arendt, A., and Hock, R.: A new method for deriving glacier centerlines applied to glaciers in Alaska and northwest Canada, The Cryosphere, 8, 503-519, 2014.
Koblet, T., GärtnerRoer, I., Zemp, M., and Jansson, P.: Reanalysis of multi-temporal aerial images of Storglaciären, Sweden (1959–99) – Part 1: Determination of length, area, and volume changes, Cryosphere, 4, 333-343, 2010.
Krieger, G., Moreira, A., Fiedler, H., and Hajnsek, I.: TanDEM-X: A Satellite Formation for High-Resolution SAR Interferometry, Geoscience and Remote Sensing, IEEE Transactions on, 45, 3317-3341, 2007.
Le Bris, R. and Paul, F.: An automatic method to create flow lines for determination of glacier length: A pilot study with Alaskan glaciers, Computers & Geosciences, 52, 234-245, 2013.
Leclercq, P. W., Oerlemans, J., Basagic, H. J., Bushueva, I., Cook, A., and Le Bris, R.: A data set of worldwide glacier length fluctuations, The Cryosphere, 8, 659-672, 2014.
Li, J., Zhen, B., and Yang, X.: The glaciers of Xizang (Tibet), Science Press, Chinese Academy of Sciences, Beijing, 1986.
Li, L., Yang, S., Wang, Z., Zhu, X., and Tang, H.: Evidence of warming and wetting climate over the Qinghai-Tibet Plateau, Arctic Antarctic & Alpine Research, 42, 449-457, 2010.
Li, X., Cheng, G., Jin, H., Kang, E., Che, T., Jin, R., Wu, L., Nan, Z., Wang, J., and Shen, Y.: Cryospheric change in China, Global and Planetary Change, 62, 210-218, 2008.
Li, X., Yang, T., and Ji, Q.: Study on Glacier Variations in the Gangrigabu Range, Research of Soil and Water Conservation, 21, 233-237, 2014.
Liu, S., Shangguan, D., Ding, Y., Han, H., Xie, C., Zhang, Y., Li, J., Wang, J., and Li, G.: Glacier changes during the past century in the Gangrigabu mountains, southeast Qinghai–Xizang (Tibetan) Plateau, China, Annals of Glaciology, 43, 187-193, 2006.
Liu, W., Guo, Q., and Wang, Y.: Temporal-spatial climate change in the last 35 years in Tibet and its geo-environmental consequences, Environmental geology, 54, 1747-1754, 2008.
Liu, X., Cheng, Z., Yan, L., and Yin, Z.-Y.: Elevation dependency of recent and future minimum surface air temperature trends in the Tibetan Plateau and its surroundings, Global and Planetary Change, 68, 164-174, 2009.
Mi, D., Xie, Z., Luo, R., and Feng, Q.: Glacier inventory of China XI. The Ganga Drainage basin. , Xi'an Cartographic Publishing House, Xi'an, 2002.
Nakawo, M. and Young, G. J.: Field Experiments to Determine the Effect of a Debris Layer on Ablation of Glacier Ice, Annals of Glaciology, 2, 85-91, 1981.
Neckel, N., Braun, A., Kropáček, J., and Hochschild, V.: Recent mass balance of Purogangri ice cap, central Tibetan Plateau, by means of differential X-band SAR interferometry, Cryosphere, 7, 1623-1633, 2013a.
Neckel, N., Braun, A., Kropáček, J., and Hochschild, V.: Recent mass balance of the Purogangri Ice Cap, central Tibetan Plateau, by means of differential X-band SAR interferometry, Cryosphere, 7, 1623-1633, 2013b.
Neckel, N., Kropáček, J., Bolch, T., and Hochschild, V.: Glacier mass changes on the Tibetan Plateau 2003–2009 derived from ICESat laser altimetry measurements, Environmental research letters, 9,

014009, 2014.
Nuimura, T., Sakai, A., Taniguchi, K., Nagai, H., Lamsal, D., Tsutaki, S., Kozawa, A., Hoshina, Y., Takenaka, S., and Omiya, S.: The GAMDAM Glacier Inventory: a quality controlled inventory of Asian glaciers, Cryosphere, 9, 849-864, 2015.
Nuth, C. and Käab, A.: Co-registration and bias corrections of satellite elevation data sets for quantifying glacier thickness change, The Cryosphere, 5, 271-290, 2011.
Oerlemans, J.: Quantifying global warming from the retreat of glaciers, Science, 264, 243-244, 1994.
Paul, F., Barrand, N. E., Baumann, S., Berthier, E., Bolch, T., Casey, K., Frey, H., Joshi, S. P., Konovalov, V., and Bris, R. L.: On the accuracy of glacier outlines derived from remote-sensing data, Annals of Glaciology, 54, 171-182, 2013.
Paul, F., Barry, R. G., Cogley, J. G., Frey, H., Haeberli, W., Ohmura, A., Ommanney, C. S. L., Raup, B., Rivera, A., and Zemp, M.: Recommendations for the compilation of glacier inventory data from digital sources, Annals of Glaciology, 50, 119-126, 2009.
Paul, F. and Haeberli, W.: Spatial variability of glacier elevation changes in the Swiss Alps obtained from two digital elevation models, Geophysical Research Letters, 35, 189-203, 2008.
Paul, F., Kaeaeb, A., and Maisch, M.: Comparison of TM Derived Glacier Areas With Higher Resolution Data Sets, EARSeL eProceedings 2, 2, 15-21, 2003.
Paul, F. and Svoboda, F.: A new glacier inventory on southern Baffin Island, Canada, from ASTER data: II. Data analysis, glacier change and applications, Annals of Glaciology, volume 50, 22-31, 2010.
Pellicciotti, F., Stephan, C., Miles, E., Herreid, S., Immerzeel, W. W., and Bolch, T.: Mass-balance changes of the debris-covered glaciers in the Langtang Himal, Nepal, from 1974 to 1999, Journal of Glaciology, 61, 373-386, 2015.
Pfeffer, W. T., Arendt, A. A., Bliss, A., Bolch, T., Cogley, J. G., Gardner, A. S., Hagen, J. O., Hock, R., Kaser, G., and Kienholz, C.: The Randolph Glacier Inventory: a globally complete inventory of glaciers, Journal of Glaciology, 60, 537-552, 2014.
Pieczonka, T., Tobias, B., Wei, J., and Liu, S.: Heterogeneous mass loss of glaciers in the Aksu-Tarim Catchment (Central Tien Shan) revealed by 1976 KH-9 Hexagon and 2009 SPOT-5 stereo imagery, Remote Sensing of Environment, 130, 233-244, 2013.
Pu, J., Yao, T., and Duan, K.: An observation on surface ablation on the Yangbark glacier in the Muztagata Ata, China, Journal of Glaciology & Geocryology, 25, 680-684, 2003.
Qin, J., Yang, K., Liang, S., and Guo, X.: The altitudinal dependence of recent rapid warming over the Tibetan Plateau, Climatic Change, 97, 321-327, 2009.
Rabus, B., Eineder, M., Roth, A., and Bamler, R.: The shuttle radar topography mission—a new class of digital elevation models acquired by spaceborne radar, Isprs Journal of Photogrammetry & Remote Sensing, 57, 241-262, 2003.
Racoviteanu, A. E., Paul, F., Raup, B., Khalsa, S. J. S., and Armstrong, R.: Challenges and recommendations in mapping of glacier parameters from space: results of the 2008 Global Land Ice Measurements from Space (GLIMS) workshop, Boulder, Colorado, USA, Annals of Glaciology, 50, 53-69, 2009.
Rosen, P. A., Hensley, S., Joughin, I. R., Li, F. K., Madsen, S. N., Rodriguez, E., and Goldstein, R. M.: Synthetic aperture radar interferometry, Proceedings of the IEEE, 88, 333-382, 2000.
Sakai, A. and Fujita, K.: Formation conditions of supraglacial lakes on debris-covered glaciers in the Himalaya, Journal of Glaciology, 56, 177-181, 2010.
Shangguan, D., Liu, S., Ding, Y., Zhang, Y., Li, J., Li, X., and Wu, Z.: Changes in the elevation and

extent of two glaciers along the Yanglonghe river, Qilian Shan, China, Journal of Glaciology, 56, 309-317, 2010.
Shangguan, D. H., Bolch, T., Ding, Y. J., Kröhnert, M., Pieczonka, T., Wetzel, H. U., and Liu, S. Y.: Mass changes of Southern and Northern Inylchek Glacier, Central Tian Shan, Kyrgyzstan, during ∼1975 and 2007 derived from remote sensing data, Cryosphere, 9, 703-717, 2015.
Shi, Y., Huang, M., and Ren, B.: An introduction to the glaciers in China, Science Press, Beijing, 1988.
Shi, Y., Huang, M., Yao, T., and He, Y.: Glaciers and Related Environments in China, Science Press, 2008a.
Shi, Y., Liu, C., Wang, Z., Liu, S., and Ye, B.: Concise glacier inventory of China, Shanghai Popular Science Press, 2008b.
Shi, Y. and Liu, S.: Estimation on the response of glaciers in China to the global warming in the 21st century, Chinese Science Bulletin, 45, 668-672, 2000.
Shi, Y., Liu, S., Shangguan, D., Li, D., Ye, B., and Shen, Y.: Two peculiar phenomena of climatic and glacial variations in the Tibetan Plateau, Advances in Climate Change Research, 2, 154-160, 2006.
Su, Z., Zhao, J., and Zheng, B.: Distribution and features of the glaciers' ELAs and the decrease of ELAsduring the Last Glaciation in China, Journal of Glaciology and Geocryology, 36, 9-19, 2014.
Sun, M., Liu, S., Yao, X., Guo, W., and Xu, J.: Glacier changes in the Qilian Mountains in the past half century: Based on the revised First and Second Chinese Glacier Inventory, ACTA GEOGRAPHICA SINICA, 70, 1402-1414, 2015.
Surdyk, S.: Using microwave brightness temperature to detect short-term surface air temperature changes in Antarctica: An analytical approach, Remote Sensing of Environment, 80, 256-271, 2002.
Wang, S., Zhang, M., Li, Z., Wang, F., Li, H., Li, Y., and Huang, X.: Response of glacier area variation to climate change in chinese Tianshan Mountains in the past 50 years, ACTA GEOGRAPHICA SINICA, 66, 38-46, 2011.
Wei, J., Liu, S., Guo, W., Xu, J., Bao, W., and Shangguan, D.: Changes in glacier volume in the north bank of the Bangong Co Basin from 1968 to 2007 based on historical topographic maps, SRTM, and ASTER stereo images, Arctic, Antarctic, and Alpine Research, 47, 301-311, 2015a.
Wei, J., Liu, S., Guo, W., Yao, X., Xu, J., Bao, W., and Jiang, Z.: Surface-area changes of glaciers in the Tibetan Plateau interior area since the 1970s using recent Landsat images and historical maps, Annals of Glaciology, 55, 213-222, 2014.
Wei, J., Liu, S., Xu, J., Guo, W., Bao, W., Shangguan, D., and Jiang, Z.: Mass loss from glaciers in the Chinese Altai Mountains between 1959 and 2008 revealed based on historical maps, SRTM, and ASTER images, Journal of Mountain Science, 12, 330-343, 2015b.
Werner, C., Wegmüller, U., Strozzi, T., and Wiesmann, A.: Gamma SAR and interferometric processing software, 2000, 1620.
Wu, K., Liu, S., Bao, W., and Wang, R.: Monitoring Glacier Change Based on Remote Sensing in the Gangrigabu Range, Southeast Tibetan Plateau, From 1980-2015, Journal of Glaciology and Geocryology, 2016a. 2016a.
Wu, K., Liu, S., Guo, W., Wei, J., Xu, J., Bao, W., and Yao, X.: Glacier change in the western Nyainqentanglha Range, Tibetan Plateau using historical maps and Landsat imagery: 1970-2014, Journal of Mountain Science, 13, 1358-1374, 2016b.
Xu, J., Liu, S., Zhang, S., Guo, W., and Wang, J.: Recent changes in glacial area and volume on Tuanjiefeng peak region of Qilian Mountains, China, PLoS One, 8, e70574, 2013.

Yang, K., Wu, H., Qin, J., Lin, C., Tang, W., and Chen, Y.: Recent climate changes over the Tibetan Plateau and their impacts on energy and water cycle: A review, Global & Planetary Change, 112, 79-91, 2014.

Yang, W., Yao, T., Xu, B., Ma, L., Wang, Z., and Wan, M.: Characteristics of recent temperate glacier fluctuations in the Parlung Zangbo River basin,southeast Tibetan Plateau, Chinese Science Bulletin, 55, 2097-2102, 2010.

Yang, W., Yao, T. D., Xu, B. Q., Wu, G. J., Ma, L. L., and Xin, X. D.: Quick ice mass loss and abrupt retreat of the maritime glaciers in the Kangri Karpo Mountains, southeast Tibetan Plateau, Chinese Science Bulletin, 53, 2547-2551, 2008.

Yao, T., Thompson, L., Yang, W., Yu, W., Gao, Y., Guo, X., Yang, X., Duan, K., Zhao, H., and Xu, B.: Different glacier status with atmospheric circulations in Tibetan Plateau and surroundings, Nature Climate Change, 2, 663-667, 2012a.

Yao, X., Liu, S., Guo, W., Huai, B., Sun, M., and Xu, J.: Glacier change of Altay Mountain in China from 1960 to 2009--Based on the Second Glacier Inventory of China, Journal of Natural Resources, 27, 1734-1745, 2012b.

Yao, X., Liu, S., zhu, Y., Gong, P., An, L., and Li, X.: Design and implementation of an automatic method for deriving glacier centerlines based on GIS, Journal of Glaciology and Geocryology, 37, 1563-1570, 2015.

Ye, Q., Bolch, T., Naruse, R., Wang, Y., Zong, J., Wang, Z., Zhao, R., Yang, D., and Kang, S.: Glacier mass changes in Rongbuk catchment on Mt. Qomolangma from 1974 to 2006 based on topographic maps and ALOS PRISM data, Journal of Hydrology, 530, 273-280, 2015.

You, Q., Kang, S., Pepin, N., Flügel, W.-A., Yan, Y., Behrawan, H., and Huang, J.: Relationship between temperature trend magnitude, elevation and mean temperature in the Tibetan Plateau from homogenized surface stations and reanalysis data, Global and Planetary Change, 71, 124-133, 2010.

Zhang, Y., Fujita, K., Liu, S., Liu, Q., and Nuimura, T.: Distribution of debris thickness and its effect on ice melt at Hailuogou glacier, southeastern Tibetan Plateau, using in situ surveys and ASTER imagery, Journal of Glaciology, 57, 1147-1157, 2011.

Zhang, Z., Liu, S., Wei, J., Xu, J., Guo, W., Bao, W., and Jiang, Z.: Mass Change of Glaciers in Muztag Ata-Kongur Tagh, Eastern Pamir, China from 1971/76 to 2013/14 as Derived from Remote Sensing Data, PloS one, 11, 2016a.

Zhang, Z., Xu, J.-l., Liu, S.-y., Guo, W.-q., Wei, J.-f., and Feng, T.: Glacier changes since the early 1960s, eastern Pamir, China, Journal of Mountain Science, 13, 276-291, 2016b.

Zwally, H. J., Jun, L., Brenner, A. C., Beckley, M., Cornejo, H. G., DiMARZIO, J., Giovinetto, M. B., Neumann, T. A., Robbins, J., and Saba, J. L.: Greenland ice sheet mass balance: distribution of increased mass loss with climate warming; 2003–07 versus 1992–2002, Journal of Glaciology, 57, 88-102, 2011.

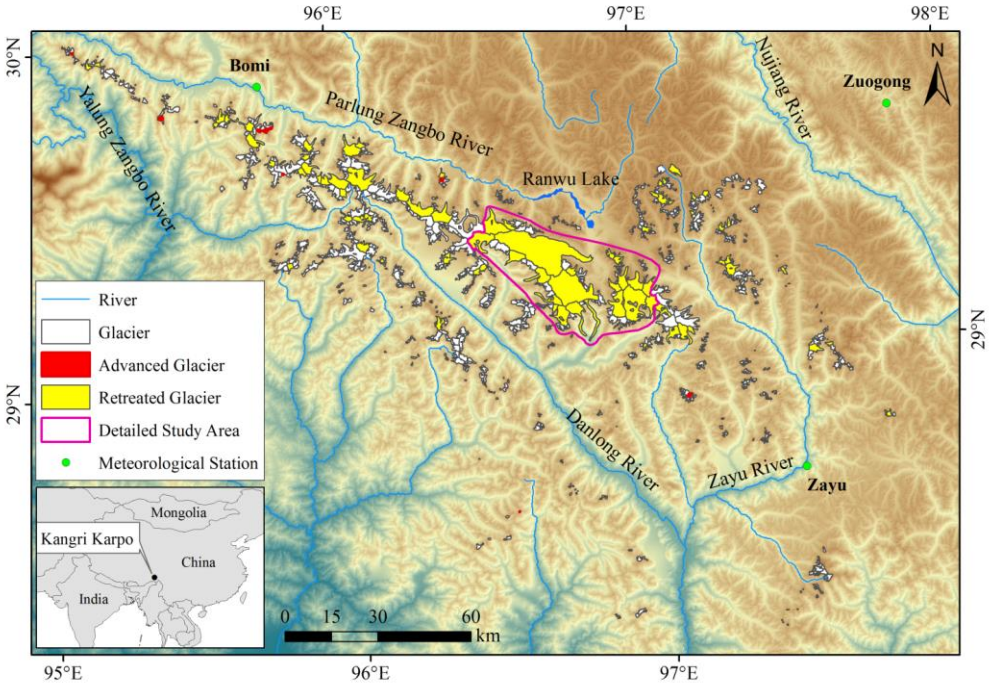

Figure 1. Overview of study area and glacier distribution, including the locations of the detailed study area and meteorological stations. 96 glaciers were selected to generate centerlines and calculate length change, and then be distinguished into advanced glaciers and retreated glaciers.

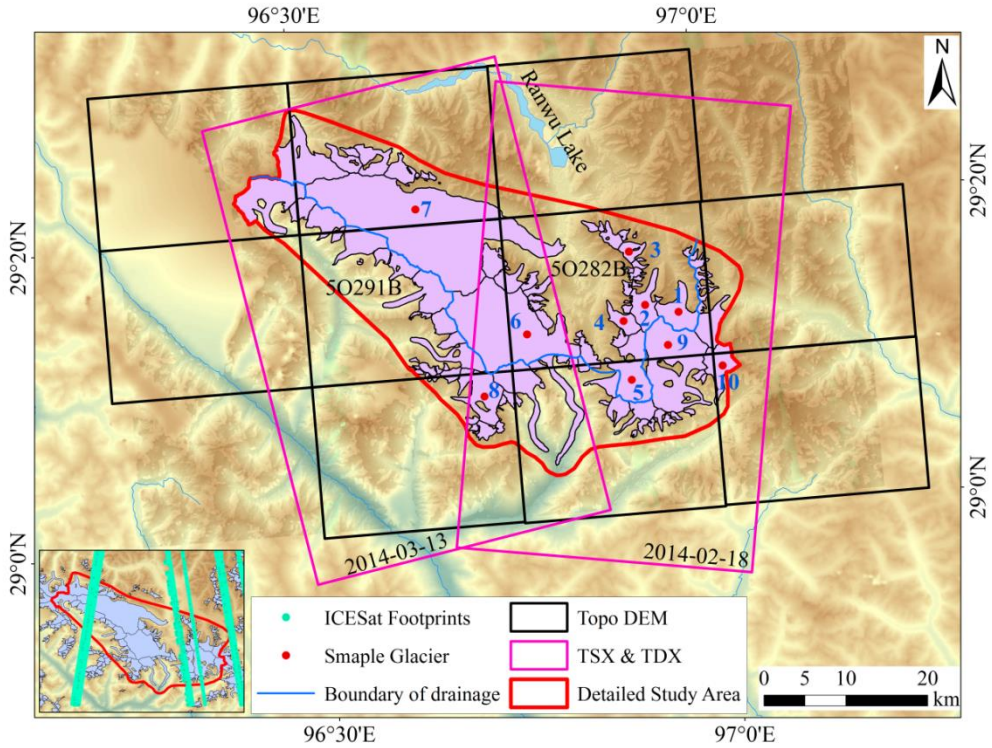

Figure 2. Location of the detailed study area, and distribution of TOPO DEMs, TSX/TDX acquisitions and ICESat footprints. Numbers indicate specific sample glaciers. 5O282B and 5O291B indicate the drainage basins, where located on north slope and south slope of the detailed study area.

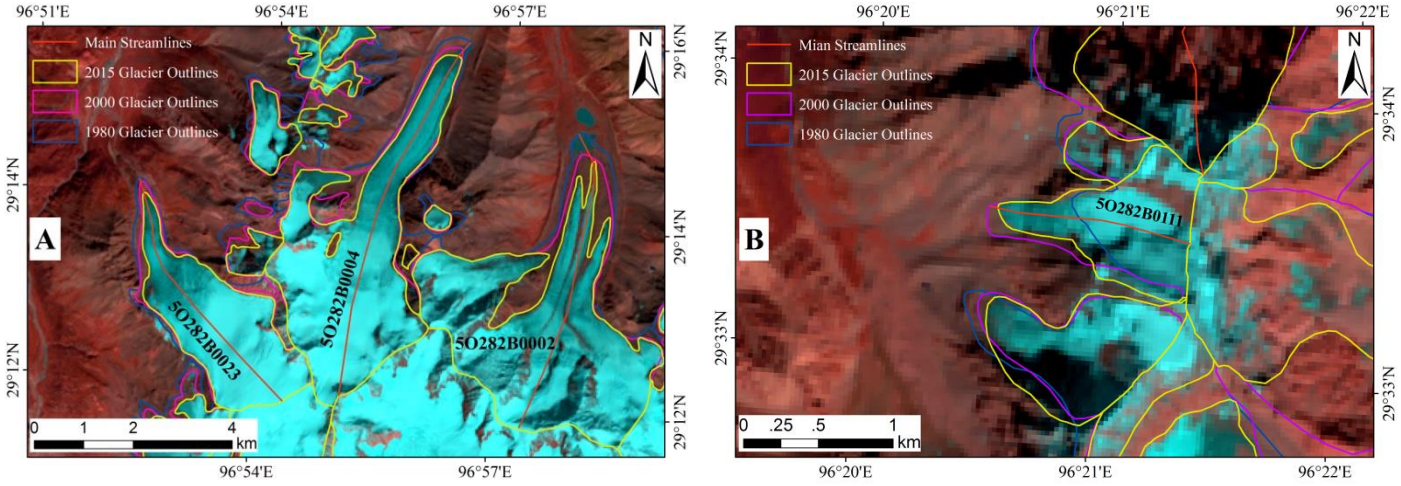

Figure 3. Example of glacier outlines derived from imagery collected in 1980, 2000s and 2015. The background image is Landsat OLI image (6 October 2015). (A) Examples of glacier retreat. (B) An example of glacier advance.

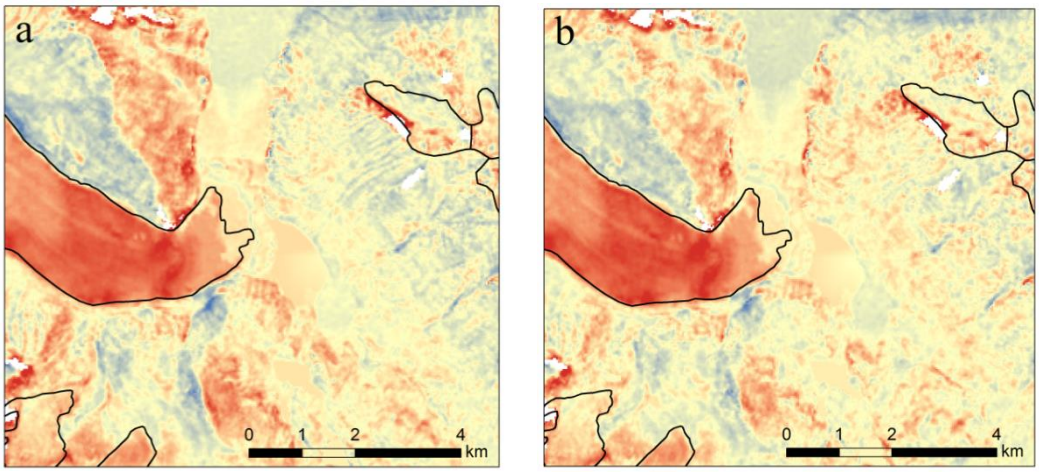

Figure 4. Elevation differences estimated between SRTM and TOPO DEM before (a) and after (b) the co-registration in the northern slope of Kangri Karpo Mountains. Location of the data example is shown in Fig. 6A.

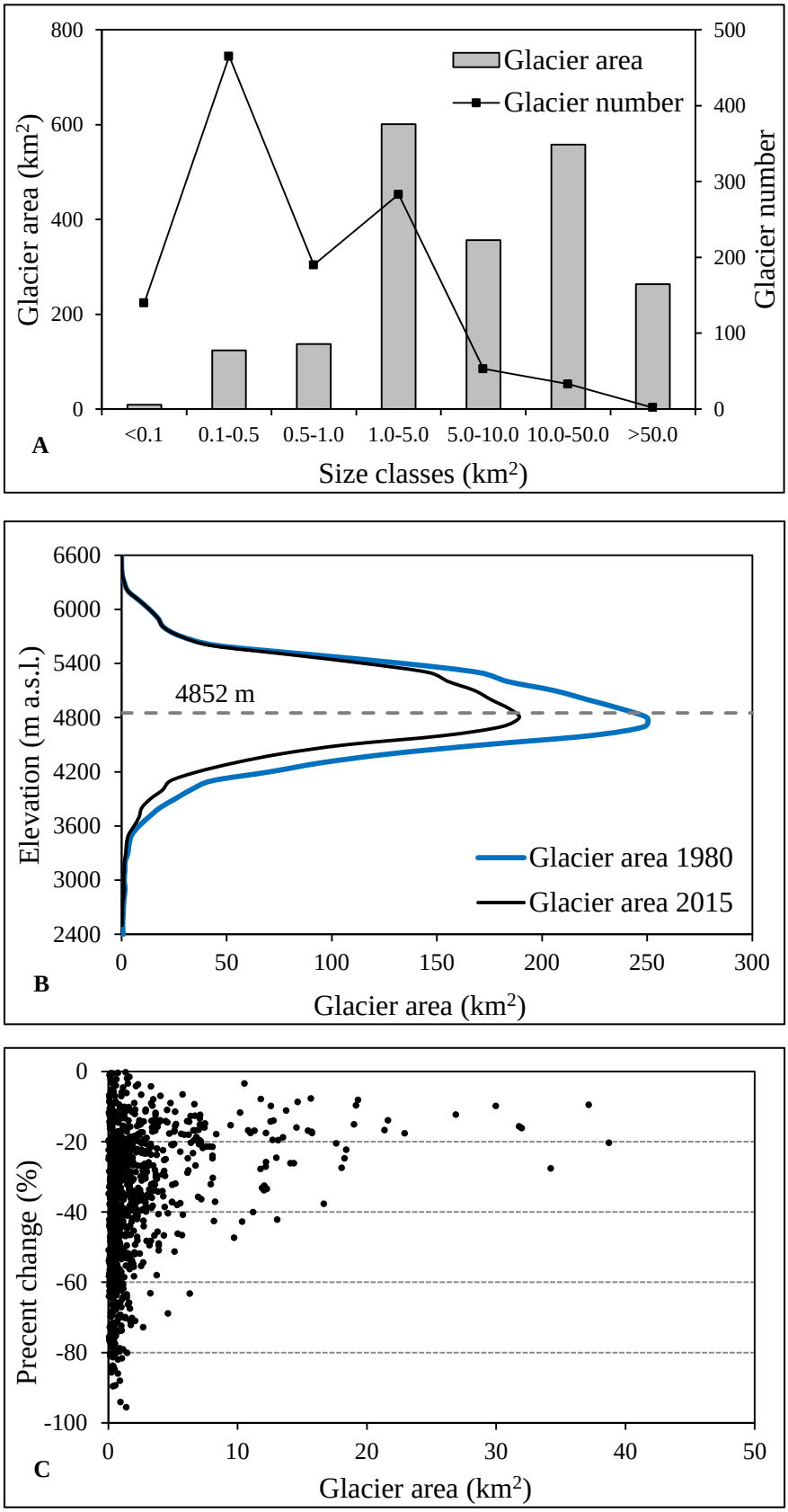

Figure 5. Glacier distribution and change in the Kangri Karpo Mountains. (A) Number and area of glaciers in different size. (B) Hypsography of glaciers in 1980 and 2015, the dashed line depicts value of median elevation. (C) Percentage changes of glaciers from 1980 – 2015.

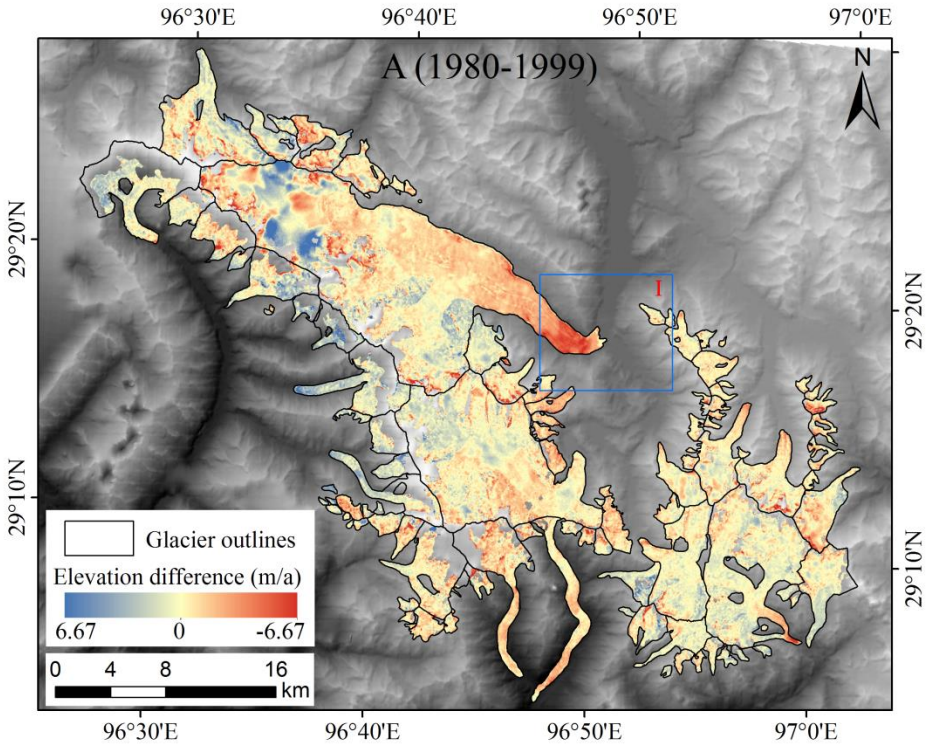
A (1980-1999)
96°30'E
96°40'E
96°50'E
97°0'E
29°20'N
29°10'N
N
I
Glacier outlines
Elevation difference (m/a)
6.67
0
-6.67
0 4 8 16
km

1

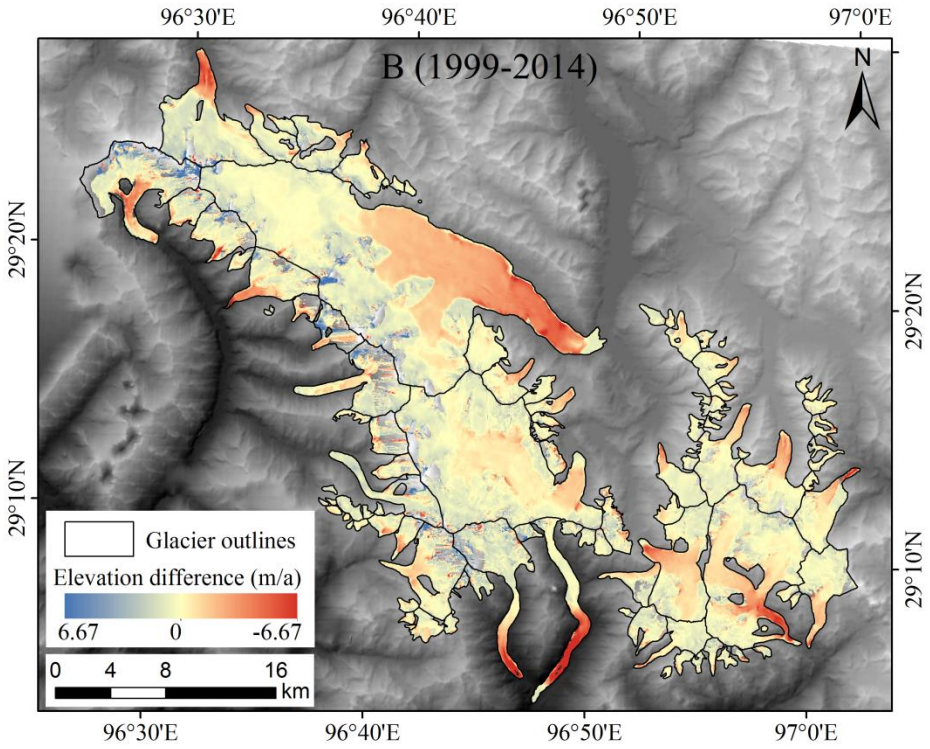
B (1999-2014)
96°30'E
96°40'E
96°50'E
97°0'E
29°20'N
29°10'N
N
Glacier outlines
Elevation difference (m/a)
6.67
0
-6.67
0 4 8 16
km

2

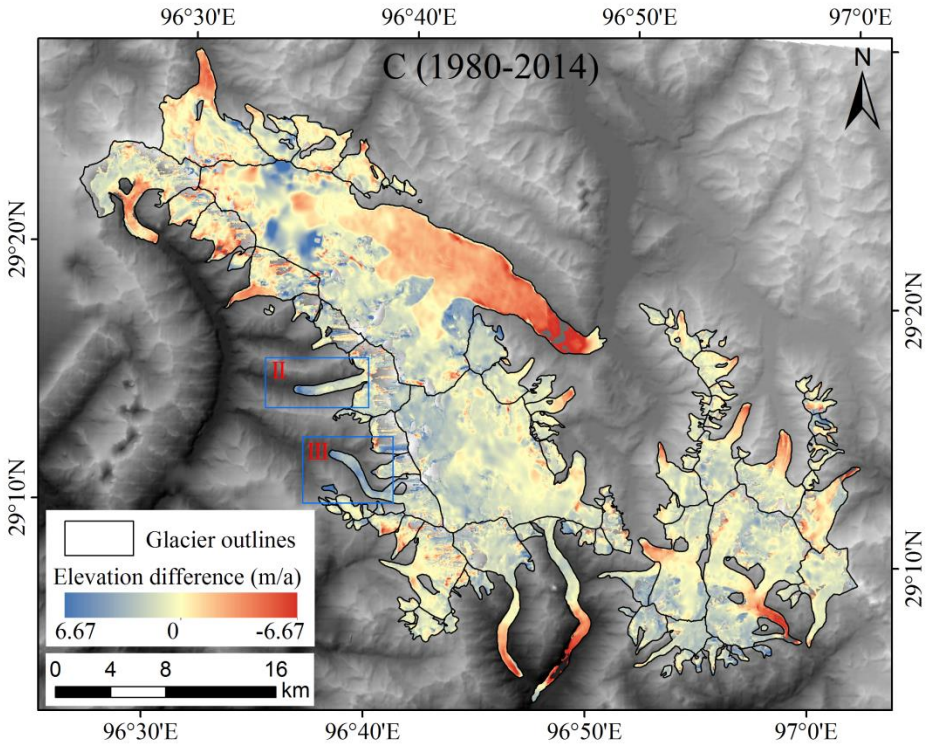

Figure 6. Elevation changes of the detailed study area of Kangri Karpo Mountains from 1980 – 2014. The glacier outlines are based on the geometric union of the 1980, 2000s and 2015 glacier extent. Ⅱ and Ⅲ are two glaciers with positive elevation changes in glacier tongue.

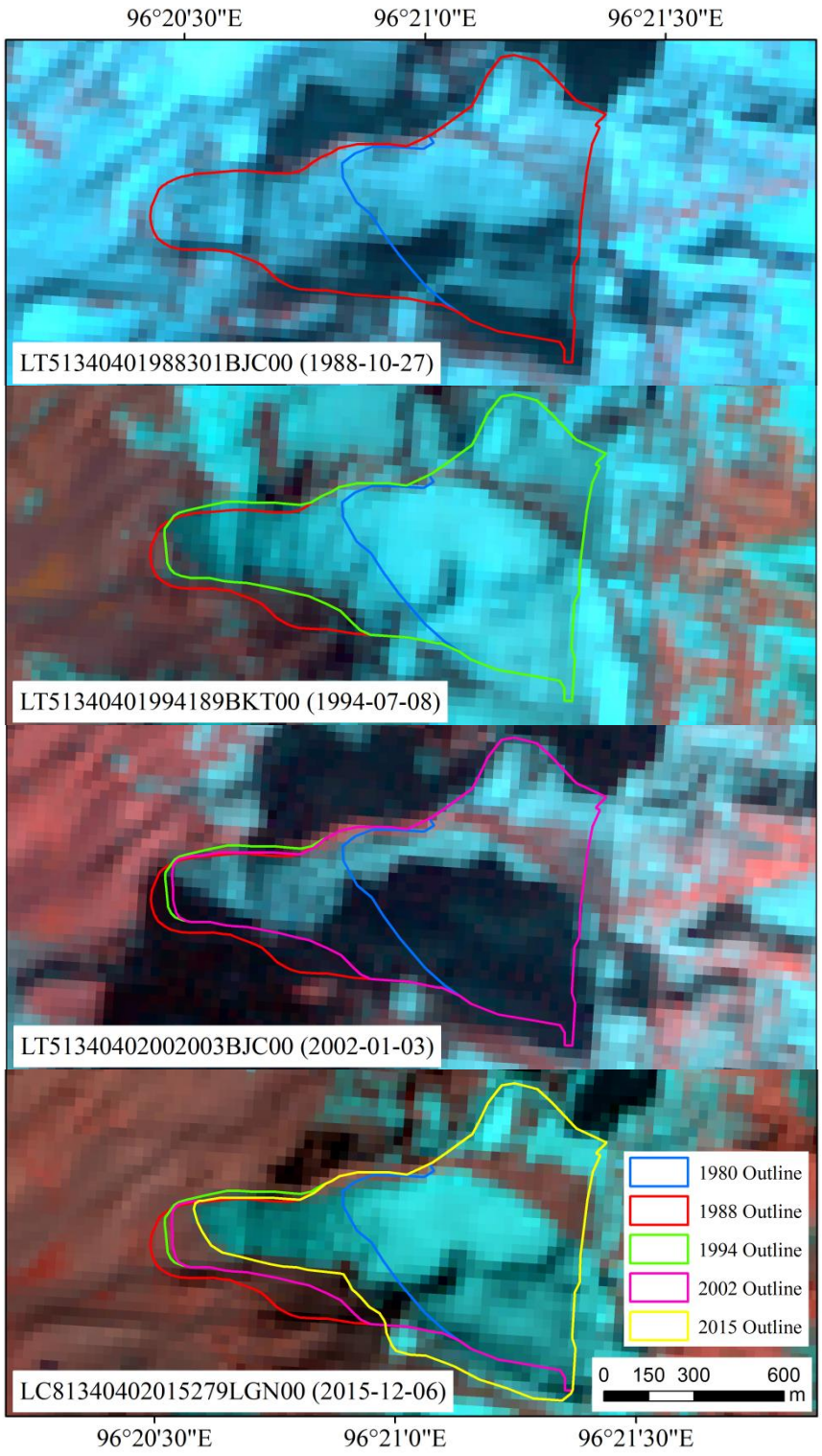

Figure 7. Terminus changes of Glacier 5O282B0111 from 1980 – 2015.

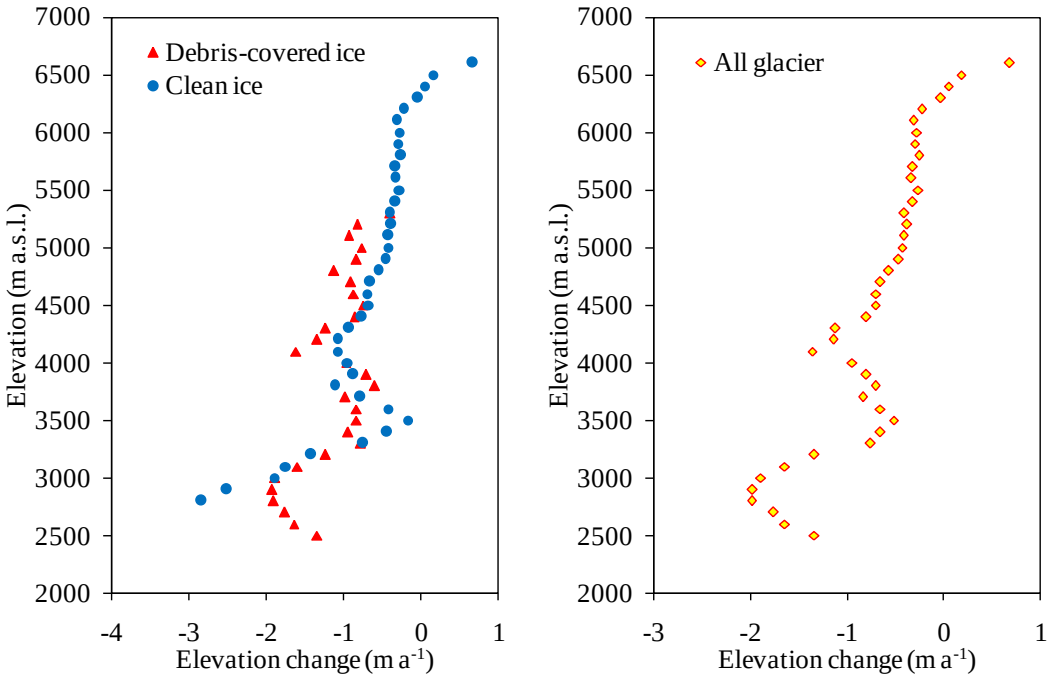

Figure 8. Glacier elevation changes at each 100 m interval by altitude in the detailed study of Kangri Karpo Mountains for the clean ice, debris-covered ice and all glaciers for the period 1980 – 2014

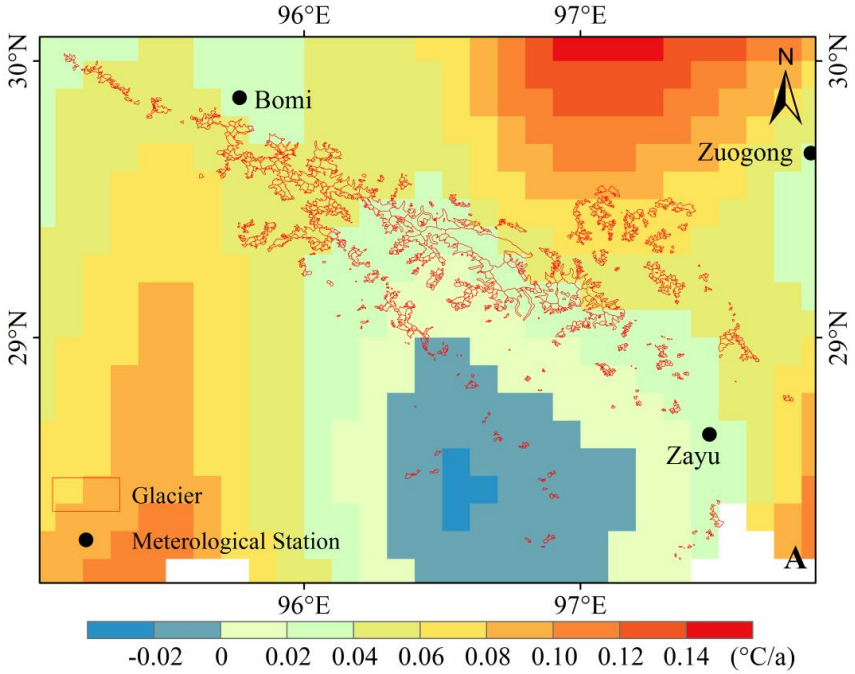

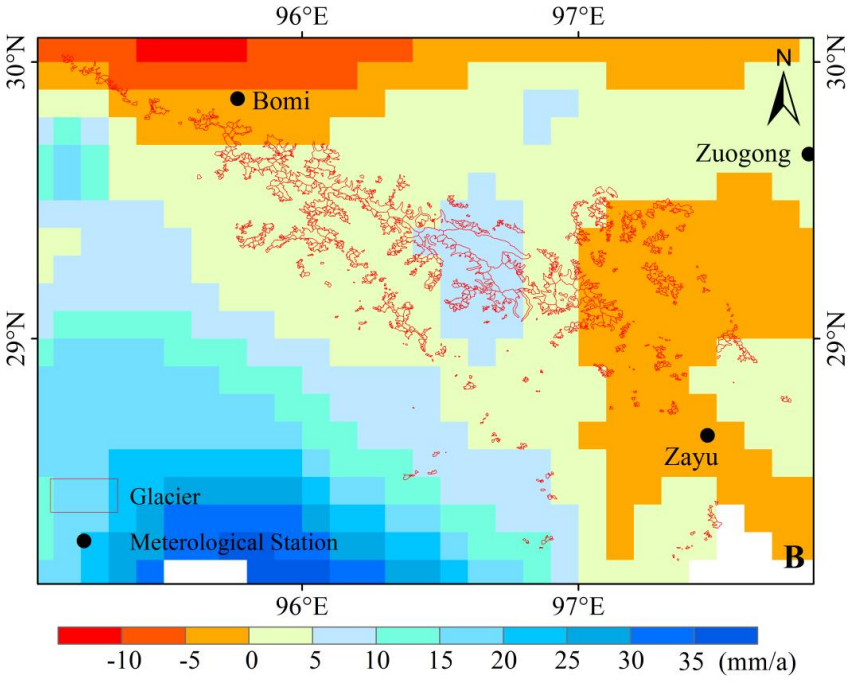

Figure 9. The changes of temperature and precipitation (from May to September) in the Kangri Karpo Mountains during 1979 – 2012. (A) temperature, (B) precipitation.

Table 1. Overview of satellite images and data sources.

Date	Source	ID	Pixel size (m)	Utilization
October 1980	Topographic Maps	-	12	Glacier identification for 1980
October 1980	TOPO DEM	H47e016002/H47e017002/ H47e018002 H47e016003/H47e017003/ H47e018003 H47e016004/H47e017004/ H47e018004 H47e016005/H47e017005/ H47e018005	30	Estimation of glacier elevation change
18 December 2001	Landsat TM	LT51340402001352BJC00	30	Validate and update the GAMDAM and CGI2 inventory
3 January 2002	Landsat TM	LT51340402002003BJC00	30	
23 October 2001	Landsat ETM+	LE71340402001296SGS00	15	
11-22 February 2000	SRTM C-band	-	30	Estimation of glacier elevation change
29 September 2015	Landsat OLI	LC81330402015272LGN00	15	Glacier identification for 2015
6 October 2015	Landsat OLI	LC81340402015279LGN00	15	
25 July 2015	Landsat OLI	LC81350392015206LGN00	15	
18 February 2014	TSX/TDX	TDM1_SAR__COS_BIST_SM_S_SRA_20140313T113609_20140313T113617	12	Estimation of glacier elevation change
13 March 2014	TSX/TDX	TDM1_SAR__COS_BIST_SM_S_SRA_20140313T113609_20140313T113617	12	

Table 2. Statistics of vertical errors between the TOPO, SRTM and TSX/TDX. MED is mean elevation difference, STDV is standard deviation, N is the number of considered pixels, SE is standard error and σ is the overall error of the derived surface elevation change.

Region	Item	MED (m)	STDV (m)	N	SE (m)	σ (m)
5O282B basin	SRTM - TOPO	-0.65	7.44	866	0.25	0.70
	TSX/TDX - SRTM	-0.90	5.83	7807	0.07	0.90
	TSX/TDX - TOPO	-1.42	5.07	7807	0.06	1.42
5O291B basin	SRTM - TOPO	0.75	8.19	963	0.26	0.80
	TSX/TDX - SRTM	0.07	12.68	8549	0.14	0.15
	TSX/TDX - TOPO	0.71	5.50	8549	0.06	0.71
Total	SRTM - TOPO	0.67	16.41	1829	0.38	0.77
	TSX/TDX - SRTM	-0.42	9.93	16356	0.08	0.43
	TSX/TDX - TOPO	-0.53	5.36	16356	0.04	0.53

Table 3. Glacier area changes in the Kangri Karpo Mountains from 1980 – 2015

Year	5O291B basin		5O291B basin		Detailed study area		Whole Mountain Range	
	Area (km^2)	Change (% a^{-1})	Area (km^2)	Change (% a^{-1})	Area (km^2)	Change (% a^{-1})	Area (km^2)	Change (% a^{-1})
1980	470.31 ± 4.82		314.28 ± 4.39		784.60 ± 5.02		2728.00 ± 34.24	
2000s	432.91 ± 6.31	-0.40 ± 0.08	287.97 ± 6.02	-0.42 ± 0.12	720.88 ± 7.20	-0.41 ± 0.06	-	-
2015	406.67 ± 6.76	-0.40 ± 0.14	254.46 ± 7.25	-0.78 ± 0.22	664.88 ± 7.83	-0.52 ± 0.10	2048.50 ± 48.65	-
1980-2015		-0.39 ± 0.05		-0.54 ± 0.08		-0.44 ± 0.03		-0.71 ± 0.06

Table 4. Area changes for ten sample glaciers in the detailed study area of Kangri Karpo Mountains.

ID	Glacier	WGI ID/ GLIMS ID	1980 Area (km^2)	1980 – 2000			2000 – 2015			1980 – 2015		
				Δa abs. (km^2)	Δa rel. (km^2)	Rate (% a^{-1})	Δa abs. (km^2)	Δa rel. (km^2)	Rate (% a^{-1})	Δa abs. (km^2)	Δa rel. (km^2)	Rate (% a^{-1})
1	Danong	5O282B0002/ G096960E29217N	15.46	-0.87	-5.6%	-0.28%	-1.74	-11.9%	-0.80%	-2.61	-16.9%	-0.48%
2	Parlung NO. 4	5O282B0004/ G096920E29228N	13.52	-1.56	-11.5%	-0.58%	-0.97	-8.1%	-0.54%	-2.53	-18.7%	-0.53%
3	Parlung NO. 10	5O282B0010/ G096904E29286N	4.98	-0.55	-11.1%	-0.55%	-0.49	-11.1%	-0.74%	-1.04	-20.9%	-0.60%
4	Zuoqiupu	5O282B0023/ G096891E29212N	7.46	-0.76	-10.2%	-0.51%	-0.43	-6.4%	-0.43%	-1.19	-15.9%	-0.45%
5	Bimaque	5O282B0025/ G096897E29157N	26.71	-1.25	-4.7%	-0.23%	-2.45	-9.6%	-0.64%	-3.70	-13.9%	-0.40%
6	Xirinongpu	5O282B0028/ G096745E29216N	98.99	-2.50	-2.5%	-0.13%	-6.21	-6.4%	-0.43%	-8.71	-8.8%	-0.25%
7	Yalong	5O282B0037/ G096657E29334N	193.43	-13.27	-6.9%	-0.34%	-7.16	-4.0%	-0.27%	-20.43	-10.6%	-0.30%
8	/	5O291B0151/ G096711E29143N	19.17	-0.42	-2.2%	-0.11%	-1.43	-7.6%	-0.51%	-1.85	-9.6%	-0.28%
9	/	5O291B0196/ G096943E29175N	56.45	-2.42	-4.3%	-0.21%	-6.11	-11.3%	-0.75%	-8.54	-15.1%	-0.43%
10	/	5O291B0200/ G097005E29155N	14.66	-0.31	-2.1%	-0.10%	-0.95	-6.6%	-0.44%	-1.26	-8.6%	-0.25%

Table 5. The length change of advanced glaciers in the Kangri Karpo Mountains. The uncertainty of glacier length in 1980 and 2015 are 6 m and 7.5 m, and the uncertainty of length change is 0.27 m a^{-1}.

WGI ID	1980		2015		Length change (m a^{-1})	Lowering of terminate elevation (m)
	Length (m)	Terminate elevation (m)	Length (m)	Terminate elevation (m)		
5O282B0111	762.75	5270	1300.87	4951	15.37	319
5O282B0223	961.93	4884	1317.09	4637	10.15	247
5O282B0225	1244.88	4705	1793.16	4483	15.67	222
5O282B0226	301.13	4870	648.43	4680	9.92	190
5O282B0278	604.73	4876	707.97	4825	2.95	51
5O283A0004	1067.55	4361	2614.65	3949	44.20	412
5O283B0022	481.76	4743	625.38	4624	4.10	119
5O291A0004	342.07	4796	798.15	4762	13.03	34
5O291B0201	4045.77	3931	5047.28	3833	28.61	98
5O291B0288	1277.50	4690	1898.78	4563	17.75	127

Table 6. The length change of glaciers in the detailed study area of Kangri Karpo Mountains. The uncertainty of glacier length in 1980, 2000s and 2015 are 6 m, 7.5 m and 7.5 m, respectively. And the uncertainty of length change during 1980 – 2000s, 2000s – 2015 and 1980 – 2015 are 0.48 m a^{-1}, 0.71 m a^{-1} and 0.27 m a^{-1}, respectively.

WGI ID	Glacier length (m)			Length change (m a^{-1})		
	1980	2000s	2015	1980 – 2000s	2000s – 2015	1980 – 2015
5O282B0002	6271.16	5773.04	5635.20	24.91	9.19	18.17
5O282B0004	7756.96	7540.24	7375.95	10.84	10.95	10.89
5O282B0010	3167.28	2970.05	2853.12	9.86	7.80	8.98
5O282B0013	3602.30	3119.71	2960.66	24.13	10.60	18.33
5O282B0017	1631.20	1394.38	1261.97	11.84	8.83	10.55
5O282B0023	5517.39	5431.23	5209.88	4.31	14.76	8.79
5O282B0025	5357.49	4834.03	4548.90	26.17	19.01	23.10
5O282B0028	16890.03	16228.66	15817.24	33.07	27.43	30.65
5O282B0034	3925.35	3860.98	3832.31	3.22	1.91	2.66
5O282B0037	32868.46	31309.45	31105.27	77.95	13.61	50.38
5O282B0081	5306.99	5212.33	4920.24	4.73	19.47	11.05
5O282B0083	8258.42	8102.68	7921.12	7.79	12.10	9.64
5O291B0104	8209.80	8075.25	7922.90	6.73	10.16	8.20
5O291B0108	7570.99	7200.65	6725.48	18.52	31.68	24.16
5O291B0113	7677.91	7627.05	7580.98	2.54	3.07	2.77
5O291B0117	15664.48	15572.74	15456.43	4.59	7.75	5.94
5O291B0150	3509.59	2677.17	2535.09	41.62	9.47	27.84
5O291B0151	6681.68	6329.14	6309.40	17.63	1.32	10.64
5O291B0179	13104.49	13037.72	12473.61	3.34	37.61	18.02
5O291B0181	15536.55	15309.66	13137.82	11.34	144.79	68.54
5O291B0196	9241.01	7157.37	6812.94	104.18	22.96	69.37
5O291B0200	7698.33	7449.66	7013.83	12.43	29.05	19.56
5O291B0372	7681.85	7236.61	6251.62	22.26	65.67	40.86

Table 7. Mean surface elevation changes and mass balance for the single glaciers and different regions in the detailed study area of Kangri Karpo Mountains from 1980 – 2014. Glacier area is the geometric union of the 1980 glacier area, 2000s glacier area and 2015 glacier area. Mean ΔH is mean surface elevation changes and Mass balance is annual mass budgets.

Region		Glacier area (km^2)	1980 – 2000		2000 – 2014		1980 – 2014	
			Mean ΔH (m)	Mass balance (m w.e. a^{-1})	Mean ΔH (m)	Mass balance (m w.e. a^{-1})	Mean ΔH (m)	Mass balance (m w.e. a^{-1})
1	5O282B0002	15.48	-11.05±0.70	-0.44±0.14	-13.33±0.91	-0.86±0.22	-20.66±1.42	-0.55±0.22
2	5O282B0004	13.63	-7.70±0.70	-0.29±0.14	-10.16±0.91	-0.65±0.22	-15.17±1.42	-0.40±0.22
3	5O282B0010	4.99	-10.31±0.70	-0.41±0.14	-10.47±0.91	-0.67±0.22	-21.44±1.42	-0.57±0.22
4	5O282B0023	7.46	-6.28±0.70	-0.23±0.14	-8.71±0.91	-0.56±0.22	-14.14±1.42	-0.37±0.22
5	5O282B0025	26.72	-4.24±0.70	-0.13±0.14	-13.72±0.91	-0.88±0.22	-14.52±1.42	-0.38±0.22
6	5O282B0028	98.99	-5.93±0.70	-0.21±0.14	-8.90±0.91	-0.57±0.22	-10.99±1.42	-0.29±0.22
7	5O282B0037	193.45	-9.21±0.70	-0.36±0.14	-15.21±0.91	-0.98±0.22	-24.51±1.42	-0.65±0.22
5O282B basin		471.05	-7.92±0.70	-0.30±0.14	11.85±0.91	-0.76±0.22	-19.13±1.42	-0.51±0.22
8	5O291B0151	19.24	-8.47±0.80	-0.33±0.16	-7.66±0.16	-0.49±0.04	-18.56±0.72	-0.49±0.11
9	5O291B0196	56.60	-3.63±0.80	-0.11±0.16	-14.33±0.16	-0.92±0.04	-15.25±0.72	-0.40±0.11
10	5O291B0200	14.66	-2.93±0.80	-0.08±0.16	-10.49±0.16	-0.67±0.04	-14.16±0.72	-0.37±0.11
5O291B basin		317.22	-4.14±0.80	-0.13±0.16	-9.74±0.16	-0.63±0.04	-14.77±0.72	-0.39±0.11
Accumulation region		530.19	-4.95±0.77	-0.22±0.16	-5.69±0.43	-0.37±0.10	-12.06±0.54	-0.32±0.08
Ablation region		258.08	-5.98±0.77	-0.27±0.16	-21.00±0.43	-1.35±0.10	-27.64±0.54	-0.73±0.08
Debris-covered region		56.87	-8.87±0.77	-0.40±0.16	-27.39±0.43	-1.76±0.10	-33.50±0.54	-0.89±0.08
Clean-ice region		731.43	-5.00±0.77	-0.23±0.16	-9.70±0.43	-0.62±0.10	-16.22±0.54	-0.43±0.08
Total		788.31	-5.30±0.77	-0.24±0.16	-11.04±0.43	-0.71±0.10	-17.46±0.54	-0.46±0.08